www.sciencemag.org/cgi/content/full/science.aae0047/DC1

Supplementary Materials for

Xist recruits the X chromosome to the nuclear lamina to enable chromosome-wide silencing

Chun-Kan Chen, Mario Blanco, Constanza Jackson, Erik Aznauryan, Noah Ollikainen, Christine Surka, Amy Chow, Patrick McDonel, Andrea Cerase, Mitchell Guttman*

*Corresponding author. E-mail: mguttman@caltech.edu

Published 4 August 2016 on *Science* Express
DOI: 10.1126/science.aae0047

This PDF file includes

Materials and Methods
Supplementary Text
Figs. S1 to S19
References

Materials and Methods

Mouse ES cell culture and Xist induction

All mouse ES cell lines were cultured in serum-free 2i/LIF medium as previously described (*7*, *11*). We used the following cell lines: (i) Male ES cells expressing Xist from the endogenous locus under control of a tet-inducible promoter (*pSM33* ES cell line, cells were kindly provided by K. Plath) as previously described (*7*). (ii) Male ES cells carrying a cDNA Xist transgene without the A-repeat integrated into the Hprt locus under control of the tet-inducible promoter (*10*) (ΔA-Xist, cells were kindly provided by A. Wutz). Xist expression was induced by treating cells (*pSM33* and ΔA-repeat deletion) with 2 μg/ml doxycycline (Sigma) for 6 hours or 16 hours depending on the assay performed. (iii) Female ES cells (F1 2-1 line, cells were kindly provided by K. Plath) derived from a 129 × castaneous F1 mouse cross. Xist expression was induced through retinoic acid induced differentiation (see below).

siRNA Transfections

For siRNA knockdown experiments, 20 nM siRNAs were transfected using the Neon transfection system (settings: 1200V, 40ms width, 1 pulse). For each transfection, two 10 μL transfections with the same siRNA were carried out in succession using 100,000 cells each, mixed, and plated equally between two poly-D-lysine (Sigma) and 0.2% gelatin (Sigma)-coated #1.5 coverslips placed into wells of a 24-well plate containing 2i media. After 48 hours, 2i media was replaced and cells on one coverslip of each pair were treated with 2 μg/mL doxycycline (Sigma) for 16 hours to induce Xist expression. Coverslips were then fixed in Histochoice (Sigma) for 10 min, washed thoroughly in PBS, and dehydrated in ethanol for storage until FISH staining.

For all proteins and non-targeting control pool, we used siRNA pool from Dharmacon (ON-TARGETplus SMARTpool siRNAs). For each cell analyzed, we ensured that the siRNA successfully reduced the targeted mRNA expression by >70%.

Retinoic acid induced differentiation in female ES cells

To initiate differentiation and Xist expression in female ES cells, we replaced 2i with MEF media (DMEM, 10% Gemini Benchmark FBS, 1x L-glutamine, 1x NEAA, 1x Pen/Strep; Life Technologies unless otherwise indicated) at 12 hours post-transfection. 24 hours after transfection, 1uM retinoic acid (Sigma) was administered for 48 hours and cells were fixed as described above. For cells not undergoing differentiation, 2i was replaced 12 hours and 48 hours after transfection.

LBR knockout female ES cells

We generated an LBR knockout in female ES cells using the CRISPR-Cas9 system. Specifically, we co-transfected a construct expressing Cas9 driven by a pCAG promoter and a pool of sgRNAs targeting an upstream and downstream region of LBR locus to delete the entire genomic locus (upstream sgRNA sequences: GGCGATGATTCAAAAGGTCG, AGCGCCGGCGATGATTCAAA, GGGCTCCGGCCTGGGCCTGC, TGAAATAAGAGAATGTTATA; downstream sgRNA sequences: TTTAACCTGTTTTTAGGTCT, AGGCTGTCTGGTCAGAATCC, CGAAGAAACCTCCCAGTCAC, CATTTTTGGTTTATTCATGG). We then picked

single colonies from transfected cells and verified LBR knockout using PCR and Sanger sequenced successful homozygous knockout lines with primers flanking deletion sites. We confirmed that this deletion leads to a complete loss of function of LBR using RNA FISH and immunofluorescence of the protein.

Integrating the BoxB aptamer sequence into Xist

We knocked in 3 copies of the viral BoxB RNA aptamer, which binds tightly to the viral λN coat protein *(38–40)*, into nucleotide 16,523 of the endogenous Xist RNA in *pSM33* ES cell line using CRISPR-mediated homologous recombination. Specifically, we co-transfected a construct expressing Cas9 driven by a pCAG promoter, a sgRNA targeting the 3' region of the Xist locus (sgRNA sequence: CCTCATCCTCATGTCTTCTC), and a single strand DNA ultramer (IDT) containing a 3x-BoxB sequence (GGGCCCTGAAGAAGGGCCCATGGGCCCTGAAGAAGGGCCCATAGGGCCCTGAAGAAGGGCCC; underlined nucleotides denote the BoxB sequence) flanked with 70 nucleotides of upstream and downstream homologous sequence of the insertion site. We then picked single colonies from transfected cells and verified BoxB integration using PCR and Sanger sequenced successful integration lines with primers flanking the integration site and confirmed correct insertion. We ensured that the Xist-BoxB was still able to silence the X chromosome by expressing it and measuring transcriptional silencing of Atrx (**Fig. S7**).

UV crosslinking

Cells were washed once with PBS and then crosslinked on ice using 0.4 Joules/cm^2 (UV4k) of UV at 254 nm in a Spectrolinker UV Crosslinker. Cells were then scraped from culture dishes, washed once with PBS, pelleted by centrifugation at 1500 × g for 4 minutes, and flash frozen in liquid nitrogen for storage at – 80 ˚C.

Immunoprecipitation and RT-qPCR

Mouse ES cells were induced then crosslinked with UV4k as described above. Pellets of 20M cells were lysed and treated with TURBO DNase (Ambion) and incubated for 10 minutes at 37 ˚C in an Eppendorf Thermomixer C to digest genomic DNA. The lysate was pre-cleared by incubation with 180 µL of Dynabeads Protein G magnetic beads (Life Technologies). Meanwhile, 10 µg of antibody for immunoprecipitation was coupled to 75 µl Protein G magnetic beads. After pre-clearing was completed, the lysate was then mixed with the appropriate antibody-coupled Protein G magnetic beads and incubated overnight at 4 ˚C on a Hulamixer sample mixer (Life Technologies) for protein capture. After immunoprecipitation, beads were washed with a wash buffer of 1× PBS with detergents and then captured nucleic acids were eluted by digesting all proteins with 5.6 U proteinase K (New England Biolabs). Eluted RNA was purified using the RNA Clean and Concentrator-5 Kit (Zymo Research) and RT-qPCR was performed as described previously (*7*) to evaluate RNA enrichment. The antibodies used for immunoprecipitation were anti-FLAG® M2 (Sigma-Aldrich; F1804) (for ΔTM- and ΔRS-LBR transfected cells), anti-SHARP (Bethyl; A301-119A), and customized LBR antibody from GenScript (LBR #4; 540774-1).

Crosslinking and Immunoprecipitation (CLIP) analysis

We crosslinked 6 hour doxycycline-induced pSM33 mouse male ES cells with 0.4 J/cm^2 of UV254. Cells were lysed and RNA was digested with RNase I to achieve a size range of 100-500 nucleotides in length. Lysate preparations were precleared by mixing with Protein G beads for 1 hr at 4C. For each CLIP sample, target proteins were immunoprecipitated from 20 million cells with 10 ug of antibody and 75 ul of Protein G beads. The antibodies were pre-coupled to the beads for 1 hr at room temperature with mixing before incubating the precleared lysate to the beads-antibody overnight at 4C. After the immunoprecipitation, the beads were washed four times with High salt wash buffer (50 mM Tris-HCl pH 7.4, 1 M NaCl, 1 mM EDTA, 1% NP-40, 0.1% SDS, 0.5% sodium deoxycholate) and four times with Wash buffer (20 mM Tris-HCl pH 7.4, 10 mM MgCl2, 0.2% Tween-20). RNAs were then eluted with NLS elution buffer (20 mM Tris-HCl pH 7.5, 10 mM EDTA, 2% N-lauroylsacrosine, 2.5 mM TCEP) with 100 mM DTT. Samples were then run through a standard SDS-PAGE gel and transferred to a nitrocellulose membrane, and a region 75 kDa above the molecular size of the protein of interest was isolated and treated with Proteinase K (NEB) followed by phenol/chloroform/isoamyl alcohol (pH 6.5) extraction to isolate the RNAs. Extracted RNAs were then purified with RNA Clean & Concentrator™-5 (Zymo). After a dephosphorylation treatment, the RNA in each sample was ligated to a mixture of barcoded adapters in which each adapter had a unique barcode identifier according to our Massively Multiplexed RNA Sequencing method (*25*). After ligation, beads were rinsed with 1x PBS and detergents and then 5x PBS and detergents prior to pooling 3-4 IPs per new tube. The proteins and RNA were then eluted from the Protein G beads with 6M urea and 40 mM DTT at 60C. Protein-RNA complexes were separated away from free RNA and the proteins were then digested with Proteinase K. From the barcoded RNA in each pool, we generated Illumina sequencing libraries as previously described(*26*).

Input samples: As a control, we sequenced an "input" RNA control for each immunoprecipitated protein. To do this, we saved 10% of the total cellular lysate prior to the immunoprecipitation step. These samples were then run through an SDS-PAGE gel alongside the immunoprecipitated sample and gel extracted from the identical region as the protein analyzed. We then made sequencing libraries from these samples as described above.

Analysis of CLIP Data

We computed and visualized the enrichment for any RNA region by normalizing the number of reads upon immunoprecipitation with a specific protein relative to the number of reads in its size-matched input control (input sample). Specifically, we counted the total number of reads overlapping the RNA region in either the immunoprecipitation sample or the input control. To account for differences in read coverage between samples, each of these numbers was normalized to the total number of reads within the same experiment. This generates a normalized score, per region, within each sample. We then computed an enrichment metric by taking the ratio of these normalized values (IP/Input).

We identified protein binding sites on the Xist RNA by identifying regions that were enriched relative to the same region in the input control ("differential enrichment")

and also was enriched relative to all other regions on the remainder of the Xist RNA ("local enrichment"). The differential enrichment accounts for biases in the size-selected input sample that would lead to a pile up of reads in specific regions of the RNA, but that do not reflect true protein binding sites. In contrast, the local enrichment accounts for cases where a given RNA might have higher overall levels of protein binding relative to the input. To compute significant enrichment, we computed the differential enrichment as defined above (IP/Input) for each window (window size=100 nucleotides). We computed the local enrichment for each region by taking the normalized number of reads for each region (IP) and dividing it by the normalized number of reads over the entire Xist RNA. To make these rates comparable, we divided each number by their respective region length prior to taking the ratio. We then generated 1,000 random permutations of the reads in the IP samples and paired input samples across the Xist RNA. For each permutation, we computed the differential and local enrichments and generated an empirical distribution of the maximum value observed for each permutation. We assigned a multiple-testing corrected p-value to each region by comparing the observed differential and local enrichment values to these permutation distributions. We identified significant windows that had a differential p-value <0.01 and a local p-value<0.01.

We identified three distinct LBR binding sites from 535-1608 nucleotides (LBS-1), 9506-10245 nucleotides (LBS-2), and 11732-11956 nucleotides (LBS-3). We also identified a SHARP binding site from 317-1056 nucleotides and PTBP1 binding site from 10859-11344 nucleotides on Xist.

Generating ΔLBS and ΔLBS-BoxB Xist

We generated ΔLBS and ΔLBS-BoxB using CRISPR-mediated knock out. To generate ΔLBS and ΔLBS-BoxB cells, mouse *pSM33* ES cells and Xist-BoxB cells were transfected with two sgRNAs flanking the LBS-1 region of Xist (sgRNA sequence: CACCGAGGAGCACAGCGGAC and TAAGGACGTGAGTTTCGCTT) and co-transfected along with the Cas9 construct described above to create a deletion of LBS-1 by non-homologous end joining. We isolated single colonies from the transfected cells for both cell lines and verified that the LBS-1 region was deleted from the genome using PCR and Sanger sequencing with primers flanking the A-repeat region of Xist. We ensured that the ΔLBS affected binding of the LBR protein using IP-qPCR and CLIP sequencing across the entire Xist RNA. We also ensured that there was no impact on SHARP binding using IP-qPCR.

dCas9-KRAB silencing

To generate stable LBR and SHARP knock down cells, we co-transfected a puromycin resistant construct expressing dCas9-KRAB driven by an Ef1a promoter and a guide RNA with scaffolding structure targeting the region near the transcription start site of LBR (sgRNA sequence: CGGGACTCCGCCGCGTG) or SHARP (sgRNA sequence: CGGTGGCGTCGGCAGCGG). Transfected cells were selected on 1 μg/mL puromycin (Sigma-Aldrich) for four days to enrich for cells that contain the dCas9-KRAB. We used FISH to verify that >90% of these puro-resistant cells had no detectable amount of mRNA after four days of puromycin selection.

LBR Protein mutagenesis

A human cDNA containing the full-length ORF of LBR was obtained from the DNASU plasmid repository as a Gateway entry clone and inserted into the pCAG-GW-λN-3xFLAG-BSD vector using an LR recombination reaction (Invitrogen). To generate ΔRS-LBR and ΔTM-LBR, λN-3xFLAG tagged full-length LBR construct was truncated using PCR-mediated deletion with primers flanking the deletion region.

Expression of cDNA rescue constructs

Mouse ES cells were electroporated using the Neon transfection system (Invitrogen) with mammalian expression vector (pCAG-GW-λN-3xFLAG-BSD vector) expressing human ΔRS-LBR, ΔTM-LBR, or full-length LBR construct from above. We knocked down endogenous LBR by treating cells with siRNAs pool from Dharmacon (ON-TARGETplus SMARTpool siRNAs) targeting only mouse LBR, but not human LBR. We ensured that the siRNAs targeted the mouse LBR specifically by ensuring that the human full-length LBR construct could rescue cells with knock down of endogenous LBR.

Generation of λN-3xFLAG epitope tagged proteins

For λN-3xFLAG-tagged protein expression and immunoprecipitation, mouse ES cells were electroporated using the Neon transfection system (Invitrogen) with mammalian expression vector (pCAG-GW-λN-3xFLAG-BSD) encoding expression of a C-terminal λN-3xFLAG tagged ORF driven by CAG. Human ORFs of GFP, LBR, EED1 and LMNB1 were obtained from the DNASU plasmid repository as Gateway entry clones and inserted into pCAG-GW-λN-3xFLAG-BSD vector using an LR recombination reaction (Invitrogen). For λN-3xFLAG-LMNB1, the LMNB1 ORF was inserted into the vector described above but with a N-terminal λN-3xFLAG tag instead (pCAG-λN-3xFLAG-GW-BSD) using an LR recombination reaction (Invitrogen). Mouse SHARP ORF was obtained by RT-PCR from *pSM33* total RNA using SHARP specific primers. The SHARP ORF was then cloned into a pENTR™/D-TOPO Gateway entry clone (Invitrogen) and inserted into the pCAG-GW-λN-3xFLAG-BSD vector as described above. Transfected cells were selected on 4 ug/mL Blasticidin (InvivoGen) to enrich for cells expressing tagged proteins. For LBR-MCP, the LBR ORF was inserted into Ef1a-GW-MCP-V5-Neo vector using an LR recombination reaction (Invitrogen) and selected with 200 ug/mL Geneticin/G418 (Invitrogen). For analysis, we used immunofluorescence staining with antibodies against 3xFLAG or V5 epitope (described below) to select for cells expressing tagged proteins.

We verified that λN-3xFLAG tagged proteins were still functional by ensuring that they could rescue knock down of the endogenous protein (**Fig. S10**).

Western blotting

pSM33 cells were lysed in buffer containing 50 mM Tris-HCl (pH 7.5), 100 mM NaCl, 1% NP-40, 0.5% sodium deoxycholate and protease inhibitor cocktail (CalBiochem; 539134) and sonicated using a Branson Sonifier at 25 watts for 20 seconds (0.7 seconds on, 3.3 seconds off) on ice. ~30 µg of total protein was separated by SDS–PAGE and transferred to nitrocellulose membranes followed by blocking with Odyssey Blocking Buffer (Licor, 927-40000). Primary antibodies were diluted in blocking buffer

as follows: anti-FLAG® M2 (Sigma-Aldrich; F1804) (1:1000), anti-lamin B receptor antibody (Abcam; ab122919) (1:1500), anti-V5 tag antibody (Abcam; ab27671) (1:1000) and anti-actin antibody (Abcam; ab3280) (1:1500). Secondary antibodies were diluted in 0.1% Tween-20 diluted in PBS as following: IRDye® 680RD Goat anti-Mouse IgG (H + L) (LI-COR; 926-68070) (1:10000) and IRDye® 800CW Goat anti-Rabbit IgG (H + L) (LI-COR; 926-32611) (1:10000). Blots were imaged with Odyssey® CLx Imager (LI-COR Biosciences) and the intensity of each band was quantified using ImageJ.

Single molecule RNA FISH

Single molecule RNA Fluorescence *in situ* hybridization (FISH) experiments were done using QuantiGene ViewRNA ISH Cell Assay (Affymetrix) and QuantiGene ViewRNA ISH Cell 740 Module (Affymetrix) according to manufacturer's protocol. Specifically, cells fixed on coverslips were first permeabilized with Detergent Solution QC at room temperature for 5 min, and then incubated with desired mixture of probe set (Affymetrix) in Probe Set Diluent QF at 40°C for 3 h, followed by incubation with PreAmplifier Mix at 40°C for 30 min, Amplifier Mix at 40°C for 30 min, and Label Probe Mix at 40°C for 30 min sequentially. For DAPI staining, coverslips were incubated in 30 nM DAPI in PBS at room temperature for 15-20 min. Probe sets and conjugated fluorophores (excitation wavelengths) for FISH were TYPE 1-XIST (550 nm), TYPE 4-GPC4, MECP2, RBMX, SMC1A (488 nm), TYPE 10-ATRX (740 nm), and TYPE 6-SHARP, LBR, LMNB1, EMD (650 nm).

Immunofluorescence and RNA FISH

For immunofluorescence (IF), cells were fixed on coverslips and permeabilized with 0.1% Triton-X in PBS at room temperature for 10 min, and blocked with 1X blocking buffer (Abcam; ab126587) or 5% normal goat serum in 0.1% Triton-X in PBS at room temperature for 30 min. Cells were then incubated with primary antibodies at room temperature for 1 h, followed by washes with 0.1% Triton-X in PBS and incubation with secondary antibodies at room temperature for 1 h. The samples were then processed using the RNA FISH protocol, as described above. Primary antibodies and the dilution used for IF were anti-Lamin B1 (Abcam; ab16048) (1:50), and anti-FLAG® M2 (Sigma-Aldrich; F3165) (1:50), and anti-Lamin B Receptor antibody (Abcam; ab122919) (1:100). Secondary antibodies and the dilution used for IF were Alexa Fluor® 488 F(ab')$_2$ fragment of goat anti-rabbit IgG (H+L) (Life Technology; 1618692) (1:100), highly x-ads DyLight® 650 goat anti-Rabbit IgG (H&L) (Bethyl; A120-201D5) (1:200), DyLight® 650 goat anti-Mouse IgG (H&L) (Bethyl; A120-201D3) (1:200), DyLight® 550 goat anti-Rabbit IgG (H&L) (Bethyl; A90-516D5) (1:200) and DyLight® 650 goat anti-Mouse IgG (H&L) (Bethyl; A90-516D3) (1:200).

X-chromosome paint

X-chromosome paint were done using MetaSystems according to manufacturer's protocol. Specifically, *pSM33* cells were fixed, permeabilized and stained with LMNB1 using the immunofluorescence procedure described above. MetaSystems DNA probes targeting X-chromosome (XMP X red) were spotted onto the samples. Samples were then denatured at 75°C for 2 minutes followed by incubation at 37°C overnight. Afterwards, samples were washed in 0.4x SSC (pH 7.0) at 72°C for 2 minutes followed by washes in

2x SSC with 0.05% Tween-20 (pH 7.0) at room temperature for 30 seconds. Samples were then rinsed briefly in distilled water, air dried and mounted in DAPI/Antifade (MetaSystems) on slides.

Microscopic Imaging

FISH, IF/FISH and X-chromosome paint samples were imaged using a Leica DMI 6000 Deconvolution Microscope with the Leica HC PL APO 63x/1.30 GLYC CORR CS2 objective. Samples stained with TYPE 10-ATRX (740 nm) were imaged using Nikon Ti Eclipse with the Nikon CFI Plan Apochromat λ DM 60x/1.40 oil objective. Images were projected with maximum projection (3 μm; step size, 0.2 μm). Samples for 3D deconvolution was imaged using Leica DMI 6000 Deconvolution Microscope with the Leica HC PL APO 63x/1.30 GLYC CORR CS2 objective (15 μm; 0.02 μm step size). 3D deconvolution images were processed using Huygens Professional (SVI; v15.05) with the built-in theoretical point spread function and the classic maximum likelihood estimation method for restoration. A manually defined signal to noise ratio value was applied for each fluorescent channel respectively. Samples stained with LMNB1 or LBR were imaged using a Zeiss LSM 880 Laser scanning confocal system with the Airyscan super-resolution module, mounted on an upright Axio Examiner Z1 microscope. We used a Plan-Apochromat 63x/1.40 NA Oil DIC f/ELYRA objective and the Airyscan module to collect super-resolution images. Single Z-section was used for these images.

X-chromosome Silencing Assay

Cells were stained for Xist RNA, Gpc4 mRNA, Atrx mRNA and siRNA-targeted mRNA by FISH and imaged. Images were then analyzed using Matlab R2013b (described below). Cells were selected if the copy number of the targeted mRNA was less than 30% of the level of the no siRNA treated cells and if they induced Xist expression. Within these cells, the copy number of Gpc4 mRNA and Atrx mRNA were quantified using a peak finding method (described below) and compared across conditions. We quantified mRNA levels for 50 individual cells. We also evaluated Xist expression in siRNA-treated cells, and observed no difference in the percentage of cells that induced Xist expression in any of the siRNA conditions relative to untreated cells.
The mean and the variance of the ratio (+Dox/-Dox) were calculated using the standard Taylor approximation method for estimating the significance of ratios. Accordingly, we calculated the average, standard deviation, and standard error of the mean as follows. The average (μ) is defined as:

$$\mu\left(\frac{+Dox}{-Dox}\right) = \frac{\mu(+Dox)}{\mu(-Dox)} + \frac{\mu(+Dox)}{\mu(-Dox)^3}\sigma^2(-Dox)$$

The standard deviation (σ^2) is defined as:

$$\sigma^2\left(\frac{+Dox}{-Dox}\right) = \frac{\sigma^2(+Dox)}{\mu(-Dox)^2} + \frac{\mu(+Dox)^2}{\mu(-Dox)^4}\sigma^2(-Dox)$$

and the standard error of the mean is defined as:

$$SEM\left(\frac{+Dox}{-Dox}\right) = \sqrt[2]{\frac{\sigma^2\left(\frac{+Dox}{-Dox}\right)}{50}}$$

Quantifying mRNAs by single molecule FISH

All image analysis was carried out using Matlab (version R2013b) utilizing built-in functions from the Image Processing toolbox. Images were first filtered using a two-dimensional median filter to remove background. Cell boundaries were outlined manually, guided by DAPI staining, to create a binary mask and applied to the various channels from the same field of view. Top-hat morphological filtering, a background subtraction method that enhances the individual focal spots, was applied to the images (*27*). The spots were then identified using a 2D peak finding algorithm that identifies local maximal signals within the cell. Once regional maxima were identified, the number of spots was counted for each cell. For better visualization of spots of mRNAs, we enhanced the spot size of the images using Fiji (ImageJ v1.51d) Maximum Filter plugin with radius of 1.0 pixel for Gpc4 and/or Atrx channel.

Calculating distance between Xist RNA compartment and Lamin B1

The nuclei of individual cells were identified manually using the DAPI staining. We identified the Xist compartment by either staining for Xist RNA (FISH) or X chromosome DNA (chromosome paint) along with immunofluorescence for Lamin B1 protein. We defined the compartment by identifying a region in the nucleus using an intensity-based threshold to partition the image within the nucleus and find contiguous 2-dimensional regions of high intensity. The threshold was determined based on Otsu method as previously described (*28*), which splits the image into 2 bins – high and low – and identifies a threshold that minimizes the variance within the partition. This creates a binary mask on the image. We visually confirmed that this binary mask accurately reflected the Xist compartment, X chromosome, or Lamin B1 region. The distance between the Xist compartment and Lamin B1 was determined by calculating the distance of each pixel between Xist or the X chromosome and Lamin B1 and finding the minimum value with a customized Fiji macro script. The area of the nucleus (Area) was measured using Fiji, and the radius of the nucleus (r) was calculated using $r = \sqrt{Area/\pi}$. We set the distance as zero if the Lamin B1 fluorescence signal overlapped with the fluorescence signal detect for Xist or the X chromosome (respectively).

Calculating distance between the Xist compartment and genomic loci

The nuclear area and Xist compartment were identified using the method described above. Genomic loci were determined by RNA FISH with probes against the intronic region of the genes using smFISH (*29*) as described above (TYPE 4-GPC4 (Intron1), NOTCH2 (Intron1) and XIST (Intron1) (488 nm)). We then identified the spot with Analyze Particle function in Fiji and selecting the spot with highest fluorescent intensity within the nucleus. We discarded the small number of images that contained more than one spot (for XIST and male ES cell GPC4) or two spots (for NOTCH2 and female ES cell GPC4). For XIST and the GPC4 locus in male cells, the distance between the Xist compartment and the locus was determined by finding the minimum distance

between Xist compartment and the locus with a customized Fiji macro script described above. For NOTCH2 and GPC4 in female ES cell, the distance between the Xist compartment and the loci was determined by calculating the minimum distance between Xist compartment and either one of the two loci. Median values and the standard error of the median were plotted in the figures. We calculated the standard error of the median as: standard error of the median = 1.2533(standard error of the mean)

We identified loci as inside the Xist compartment if the fluorescence signal of the locus overlapped with these fluorescence signal for Xist (for XIST and male ES cell GPC4) or the fluorescence signal of either one of the two loci overlapped with the fluorescence signal from the Xist compartment (for NOTCH2 and female ES cell GPC4).

RNA antisense purification (RAP) coupled with DNA sequencing

10 million mouse ES cells were induced with doxycycline for 6 , lysates were prepared, and Xist RNA was captured and purified as previously described (*7*). For Xist RNA capture, we used antisense 5' biotinylated 90-mer DNA oligonucleotides (Eurofins Operon) that spanned the entire length of the Xist RNA as previously described (*11*). To elute captured DNA, we incubated the beads with 15 U RNase H in 20 uL RNase H buffer (NEB Biolabs) at 37°C for 1 hour. The RNase H digested samples were then transferred to a new tube. To reverse crosslinks, we added 25 uL Hybridization Buffer (20 mM Tris-HCl (pH 7.5), 7 mM EDTA, 3 mM EGTA, 150 mM LiCl, 1% NP-40, 0.2% N-lauroylsarcosine, 0.125% Na-Deoxycholate, 3M Guanidinium Thiocyanate, 2.5mM TCEP), 125 uL NLS Elution Buffer (20 mM Tris-HCl (pH 7.5), 10 mM EDTA, 2% N-lauroylsarcosine, 2.5mM TCEP), 500 mM NaCl and 4 U Protease K (NEB Biolabs, Molecular Biology Grade) and incubated at 60°C overnight. Eluted DNA was sequenced, aligned and analyzed as previously described (*7*, *26*).

Aggregate gene analysis

We calculated the metaplot by first scaling the number of reads in each sample to obtain the same total number of reads for all the samples in 1 kb windows. We then normalized each sample to its own input followed by a second normalization to the wild-type Xist sample to obtain the relative ratio of each window. We then plotted the log-ratio of these values 100 Kb upstream and downstream of each gene on X-chromosome along with the gene body region, which was scaled across genes to represent the same overall area. To avoid overcounting, when we extended a given gene, we only included those extensions in our aggregation set if they were not already included in the left or right extensions from a previous gene. Genes within 5 Mb of the Xist transcription locus were excluded from the analysis because they represent outliers in terms of average Xist enrichment. The plots were generated and visualized using DeepTools and Gviz. The "active" and "inactive" genes were defined as previously described (*7*). Expression levels were split based on RPKM levels computed from chromatin RNA-Seq levels as previously described (*26*). We only considered genes with RPKM expression >1. Genes with RPKM expression >5 are grouped as highly actively transcribed genes.

The regional normalization curve was obtained by calculating a smoothed running average across a 10-kilobase window on the chromosome. Accordingly, it was included to demonstrate the overall pattern of the data, which can be more easily seen in a smoothed aggregate representation relative to overlay of each individual data point. Each

number in the plot (Wi) was calculated using the simple mean of the 1-kilobase pair windows shown in the top panel, such that:

$$W_i = \frac{W_i + W_{i+1} + \cdots + W_{i+9}}{10}$$

Supplementary Text

Note S1

We measured X chromosome expression before and after Xist induction using single molecule FISH. This approach provides more sensitive measurements relative to aggregate based methods because it allows us to analyze only cells that induce Xist expression (~50% in our system). Furthermore, it allows us to analyze individual cells that successfully deplete the target mRNA of interest (siRNA experiments) or that contain the transfected fusion proteins in our experiments. However, because of the nature of smFISH, we can only measure a few genes (rather than all genes on the X chromosome). Accordingly, we selected 5 genes that are spread across the X chromosome and that are well expressed prior to Xist induction and are normally silenced by 16 hours of Xist induction in our doxycycline-inducible system (*11*) (**Fig. S1B**). As a control, we measured the expression of two autosomal genes, which are not expected to be effected upon induction of Xist expression (**Fig. S1C**). We, and others, have previously shown that these X chromosome genes accurately reflect the transcriptional status of many genes across the inactive X chromosome (*9*, *11*).

Note S2

To measure Xist-mediated silencing, we made use of our previously developed male mouse embryonic stem (ES) cell line containing a doxycycline-inducible Xist expressed from its endogenous location (*7*). Importantly, this inducible system has been shown to represent a well-synchronized model that accurately reflects the initiation of XCI (*7*, *9*–*11*, *30*). Furthermore, this male-inducible system is more sensitive for identifying proteins that affect silencing compared to a female system because Xist-mediated silencing in males will lead to loss of 100% of X-chromosome transcripts rather than only 50% in a female system, which still retains one active X. Moreover, because this system is well synchronized, relative to differentiation induced activation, it provides more reliable measurements of silencing at a given time point.

Note S3

Among the 10 Xist-interacting proteins that we previously identified (*11*), LBR is the only protein that does not contain a canonical RNA binding domain. We hypothesized that the Arginine-Serine (RS) motif of LBR might be required for interacting with Xist because the RS motif is present within a class of mRNA binding proteins involved in splicing (SR proteins) (*31*–*33*), is overrepresented in RNA binding proteins that lack canonical RNA binding domains (*34*), and the RS motif of LBR was previously shown to interact with RNA *in vitro* (*35*).

Note S4

We explored the available literature reporting LBR mutant mice. Briefly, there are two general classes of LBR mutants that have been studied: (i) those containing naturally occurring ichthyosis (*36*) (*ic*) mutants that were subsequently mapped to mutations in the LBR gene and (ii) a gene trap truncation of LBR that leads to an in-frame fusion of the N-terminal region of LBR to a β-geo reporter (LBR-GT) (*37*).

In the case of the *ic* mutants studied, the LBR protein is truncated after the fourth transmembrane domain. These homozygous mutant mice are born at a ~50% reduced

frequency from the expected Mendelian ratio (*36*), demonstrating that LBR knockout leads to an embryonic defect. Yet, the sex distributions of live births were not reported and so it is unknown if there is a sex bias or simply ~50% penetrance of the lethality phenotype that is evenly distributed between the two sexes.

In the case of LBR-GT, there is an even more extreme skewing in live births observed (*37*). In this case, the authors characterize these embryos and demonstrate that the observed lethality occurs during pre-implantation development – the precise time when XCI occurs. While it is not clear whether there is a sex bias, there are reported live female births, which is incompatible with an XCI defect. However, this LBR-GT mutant is not a complete LBR loss-of-function because this mutant protein is still expressed and contains four transmembrane domains in addition to the fully intact RS and Lamin B1 binding domains at the N-terminus. This mutation is similar to the ΔTM mutant, which we found is sufficient for Xist binding and for the initiation of XCI in ES cells (see **Fig. S6**).

Accordingly, it is unclear how many of these reported embryonic defects in either class of mutants are specifically due to defects in XCI or other effects of LBR. Although the observed embryonic lethality is not fully penetrant, possibly because of the nature of the mutations generated, it would appear that both males and females are impacted by disruption of LBR. This is likely due to the importance of LBR and the nuclear lamina in nuclear structure and gene regulation beyond XCI. Indeed, other critical Xist interacting proteins, including SHARP, appear to be embryonic lethal in both males and females in addition to its essential role in XCI.

Future work will be needed to more fully characterize these various mouse models and to generate new conditional LBR models in order to explore the effects of these LBR mutants specifically in XCI.

Note S5

To determine where LBR binds to Xist, we UV-crosslinked RNA-protein complexes in cells, digested RNA into short fragments, immunoprecipitated LBR, gel extracted crosslinked RNA-protein complexes, and sequenced the Xist RNA (CLIP (*38–40*), see **Methods**). We identified 3 discrete LBR binding sites (LBS) that are spread across >10,000 nucleotides of the Xist RNA (**Fig. 2A**, see **Methods**). These LBR binding sites are distinct from the binding sites of other Xist interacting proteins, including SHARP and PTBP1 (**Fig. 2A**).

Note S6

To disrupt Xist-LBR binding, we generated a mutant Xist that precisely deletes a region within the LBR binding site that is not within the SHARP binding site (ΔLBS, **Fig. 2A**). In ΔLBS-Xist, LBR binding was lost across the entire Xist RNA without impacting SHARP binding (**Fig. 2B**, **Fig. S8**). The observation that deletion of a single LBR binding site leads to loss of LBR binding across Xist **(Fig. S8)** suggests that these sites might be involved in a long range structural interaction that is required for LBR binding.

Note S7

To confirm the integrity and stability of the Xist RNA in the ΔLBS-Xist truncation mutant, we performed RNA FISH using independent probes against the 5' and 3' end of Xist. In all of these various mutants, we observe a comparable expression level and localization signal in both cases. We also performed RT-qPCR using primers against the 5' and 3' end of Xist to confirm the expression level of these mutants and found that all of these mutants show comparable expression levels to the full-length Xist **(Fig. S9)**.

Note S8

In addition to localization at the nuclear lamina (*4*, *41*, *42*), previous studies have shown that the inactive X chromosome can also be localized at the nucleolus (*4*, *43*). However, this association with the nucleolus occurs during S-phase of the cell cycle during the maintenance phase of XCI (*43*). Interestingly, even in this context, the Xi is localized at the nuclear lamina in ~50% of cases (*43*). During initiation of XCI, the context we discuss here, we observe that the Xist compartment appears to be close to the nuclear lamina in virtually all cells (**Fig. 3B**), suggesting that localization at the nuclear lamina occurs at steady state.

Note S9

We selected the Gpc4 locus to measure the distance between the Xist compartment and actively transcribed genes by RNA FISH because it is located >50 megabase pairs (Mbs) away from the Xist transcription locus. We previously found that regions that are close to the Xist locus (within 5 Mbs) show higher levels of Xist localization simply because of its close linear distance (*7*). Although Atrx is also strongly depleted for Xist RNA localization by RAP-DNA, we chose to exclude Atrx from our imaging analysis because it is in close linear proximity to Xist (within 2.5 Mbs) and may therefore show higher levels of signal overlap simply because of the more limited resolution of these imaging experiments.

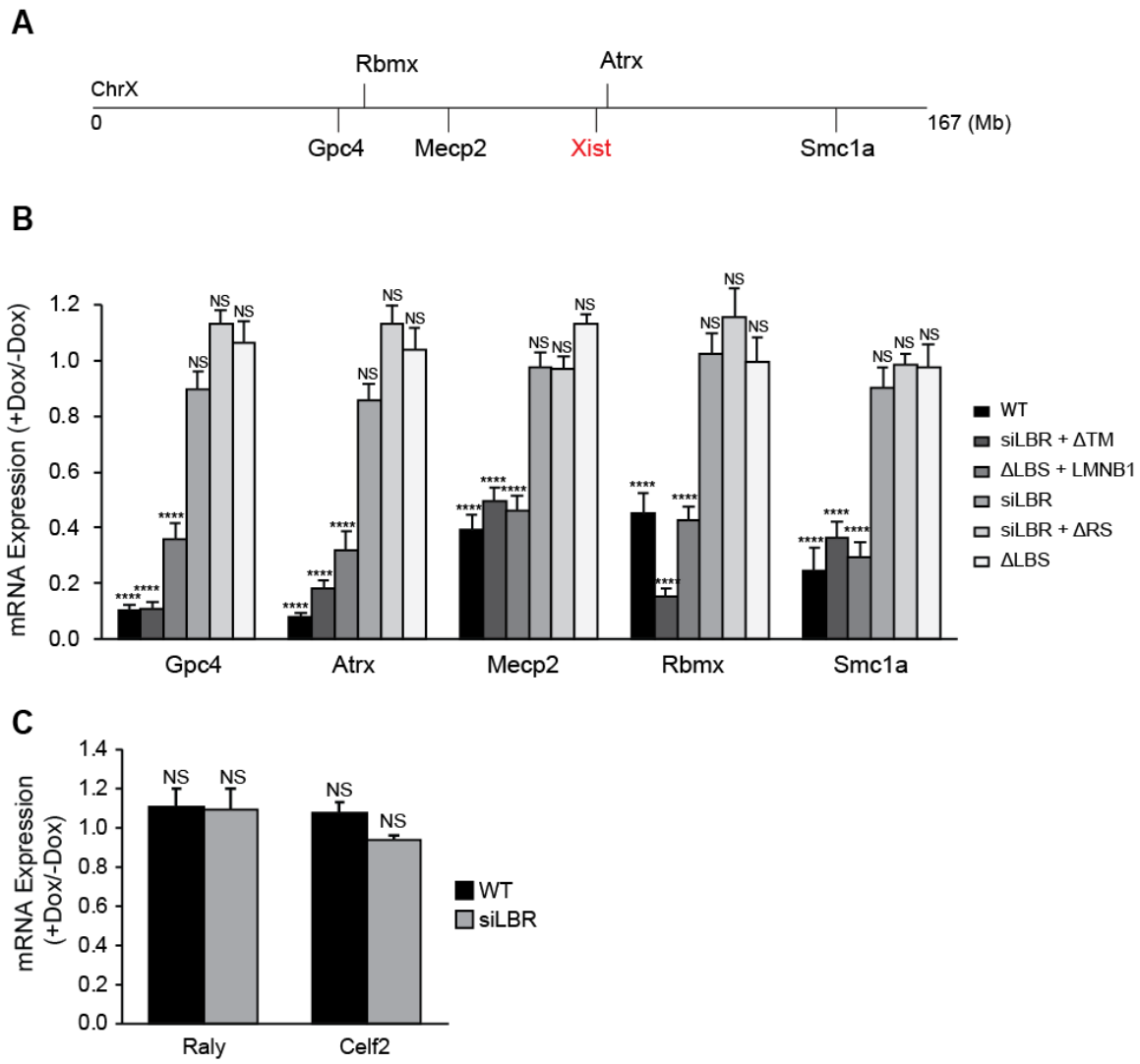

Fig. S1. Knock down of LBR abolishes Xist-mediated gene silencing of X-chromosome genes, but has no effect on autosomal genes.

(A) A diagram showing the genomic locations of Xist (red) and the other X-linked genes (black). (B) Quantification of the number of mRNA molecules present after induction of Xist normalized to the number of the mRNA molecules prior to Xist induction across different conditions for 5 different X-linked genes (Atrx, Gpc4, Rbmx, Smc1a and Mecp2). (C) Quantification of the number of mRNA molecules present after induction of Xist normalized to the number of the mRNA molecules prior to Xist induction for 2 autosomal genes (Raly and Celf2) in control samples and upon knock down of LBR. Error bars represent the standard error across 50 individual cells. NS: not significantly different from 1; **** represents values significantly different from 1 with a p-value<0.001 based on a one-sample t-test.

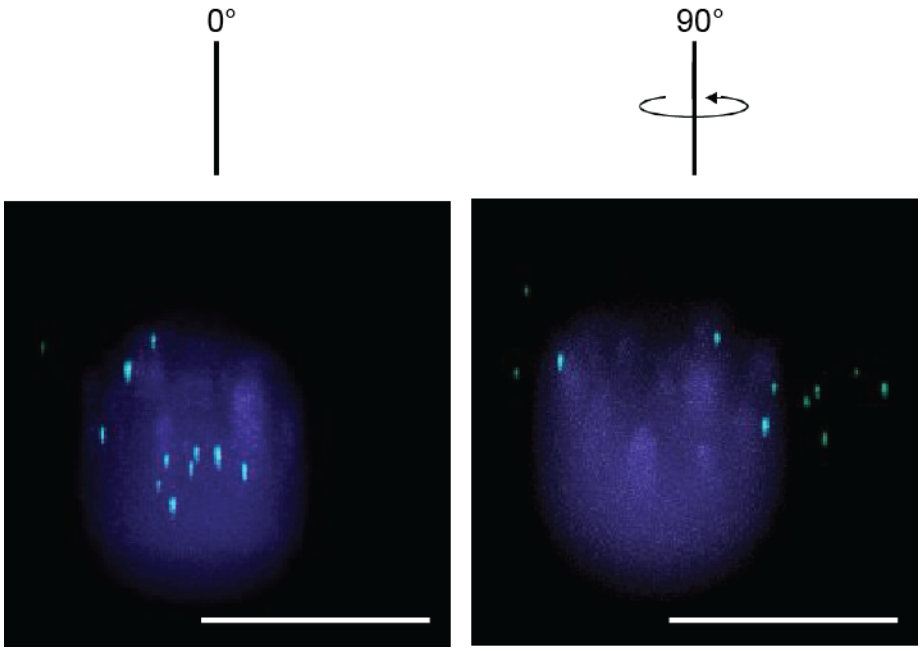

Fig. S2. 3D image deconvolution demonstrates that most Gpc4 mRNAs are localized in the cytoplasm.
3D deconvolution image of an individual cell for Gpc4 mRNAs (cyan) and nucleus (DAPI; blue). Image on the right is the 90-degree rotation of the image on the left to show that the Gpc4 mRNAs, which seems to be localized in the nucleus in the left panel, are actually localized in the cytoplasm.

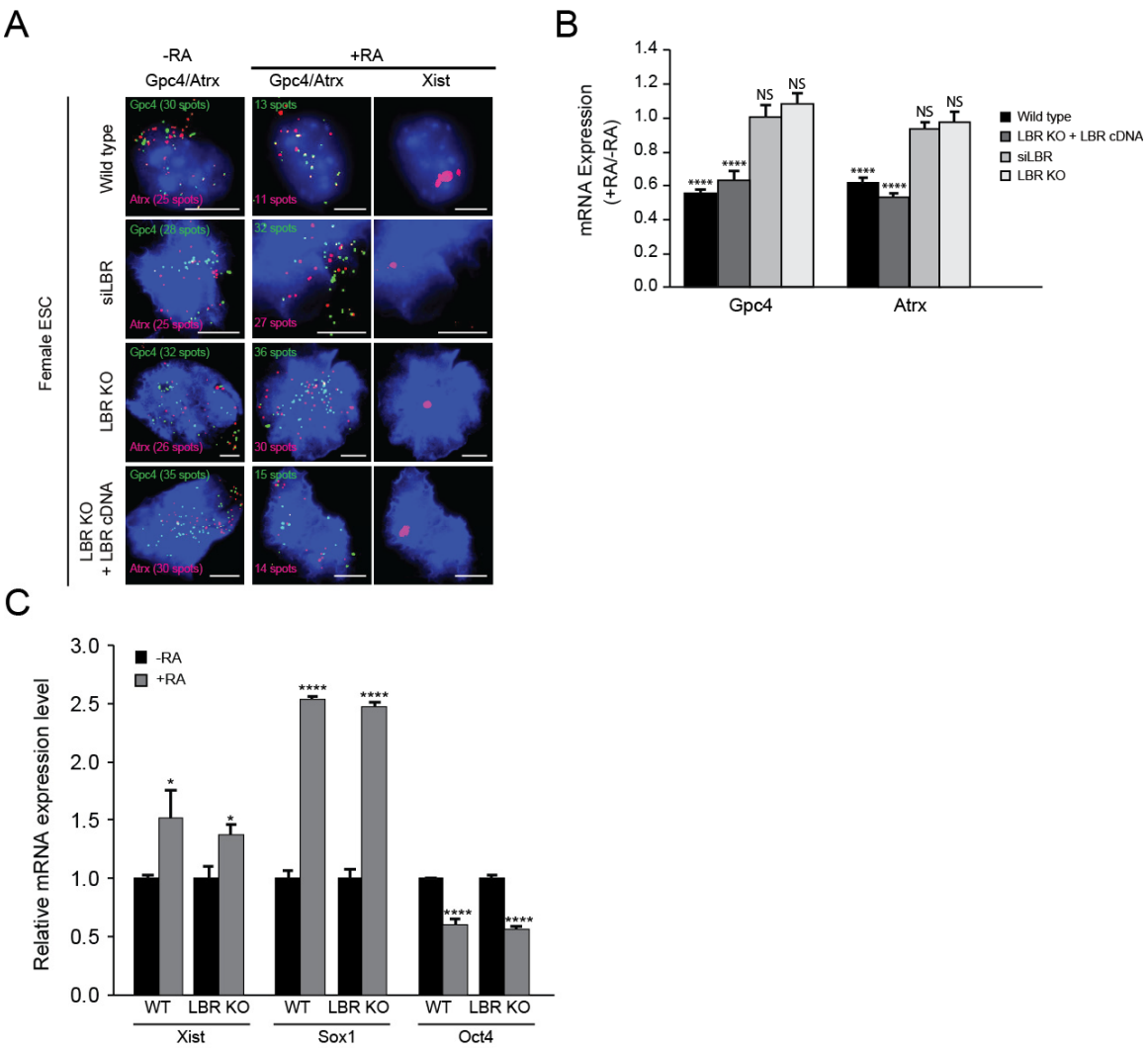

Fig. S3. LBR is required for transcriptional silencing in differentiating female ES cells.

(A) Images of individual cell showing staining of DAPI (blue), Xist (red), Gpc4 (green), and Atrx (red) upon knock down or knock out of LBR in female ES cells prior to differentiation (-RA; left) or after differentiation for 48 hours (+RA; middle and right). Scale bars: 5 micrometers. (B) Quantification of the number of Gpc4 and Atrx mRNA molecules present after differentiation normalized to the number of the mRNA molecules prior to differentiation in LBR knock down, LBR knock out, or LBR knock out cells transfected with a full length LBR cDNA in female ES cells. Knock down or knock out of LBR abolishes the Xist-mediated silencing in female ES cells, while a full-length LBR cDNA can rescue this defect in LBR knock out cells. Error bars represent the standard error across 50 individual cells. NS: not significantly different from 1; **** represents values significantly different from 1 with a p-value<0.001 based on a one-sample t-test. (C) RNA levels of Xist, differentiation marker (Sox1) and pluripotency marker (Oct4) measured by RT-qPCR in wild-type or LBR knock out female ES cells prior to differentiation (-RA) or after differentiation for 48 hours (+RA). The RNA expression level is normalized to the expression level of Gapdh RNA followed by a second normalization to the -RA cells of each sample. Error bars represent the standard error

from three independent RT-qPCR experiments. * p-value<0.05, **** p-value<0.001 relative to -RA cells by an unpaired two-sample t-test.

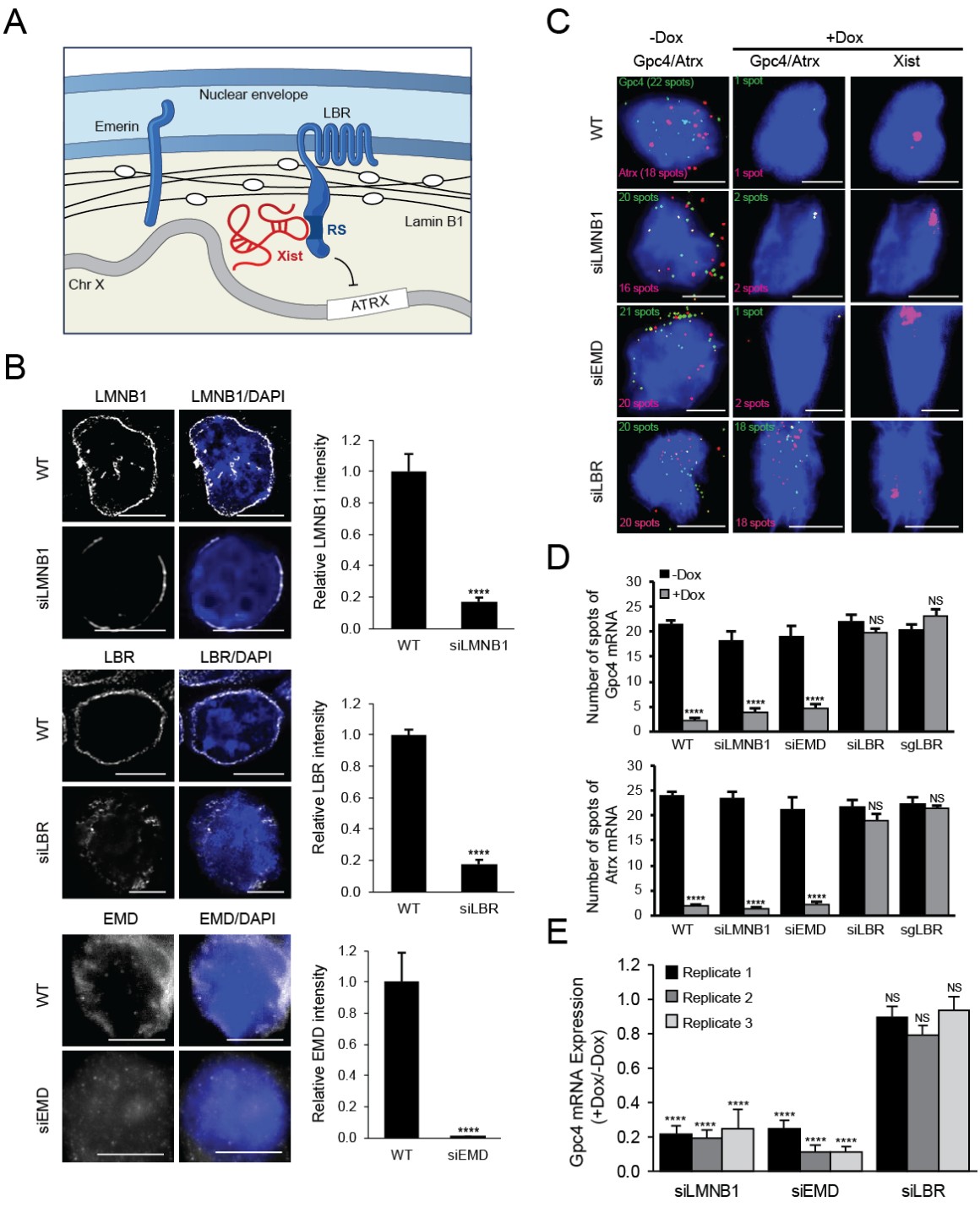

Fig. S4. Knock down of Lamin B1 or Emerin leads to loss of protein levels, but does not affect Xist-mediated silencing.
(A) A schematic of the nuclear lamina and the interaction between LBR and Xist. (B) Images and quantification of the fluorescence intensity of LMNB1, LBR, or EMD protein levels in wild-type and upon knock down with siRNAs. The fluorescence intensity of the protein (white) is normalized to the area and the fluorescence intensity of DAPI staining (blue). (C) Images of individual cell showing two X-linked mRNAs, Gpc4 (green) and

Atrx (red) along with Xist (red) and DAPI (blue) after treatment with different siRNAs (rows). The number of mRNA molecules is shown. (D) Quantification of the copy number of Gpc4 and Atrx mRNA prior to Xist induction (-Dox) and after Xist induction (+Dox) upon knockdown of various nuclear lamina proteins. WT: scrambled siRNA control. siEMD: Emerin knockdown. siLMNB1: Lamin B1 knockdown. sgLBR: Knockdown of LBR using dCas9-KRAB. NS: not significant, **** p-value<0.001 relative to –Dox cells by an unpaired two-sample t-test. (E) Three independent replicates showing the copy number of Gpc4 mRNA molecules after induction of Xist normalized to the number of the mRNA molecules prior to Xist induction upon knockdown of various nuclear lamina proteins. Error bars represent the standard error across 50 individual cells. NS: not significantly different from 1; **** represents values significantly different from 1 with a p-value<0.001 based on a one-sample t-test. Scale bars: 5 micrometers.

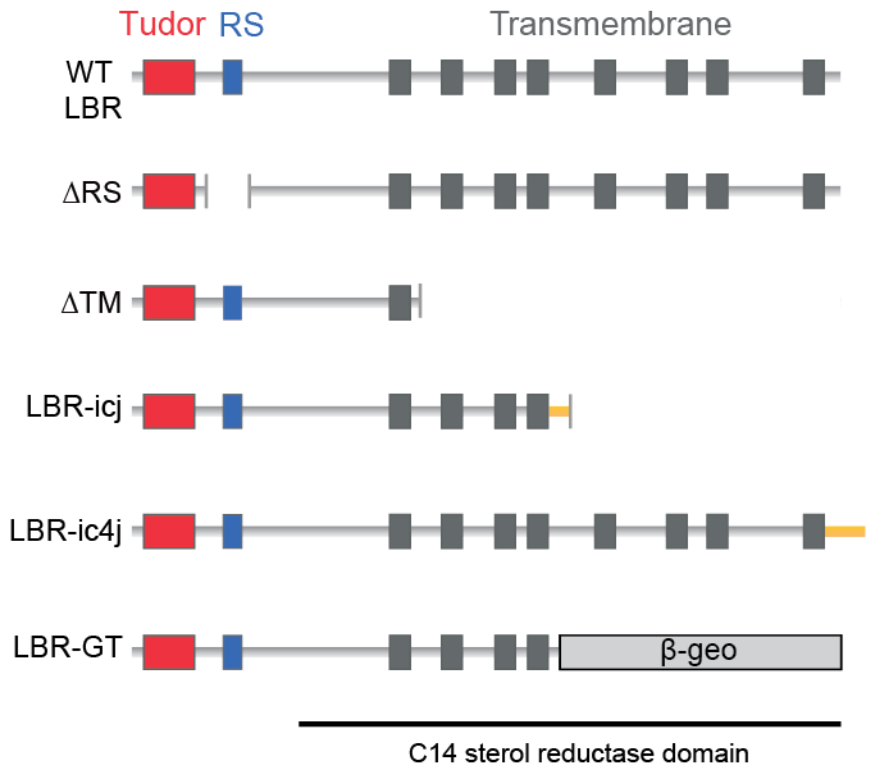

Fig. S5. The domain structure of the LBR protein and different LBR mutants. The domain structure of the LBR protein highlighting the Tudor domain (red), RS motif (blue), and 8 transmembrane domains (gray). The regions deleted in ΔRS-LBR (amino acids 71-90) and ΔTM-LBR (amino acids 237-615), and other LBR mutations generated in previous mouse models, LBR-icj (1088insCC, causing a subsequent stop codon at amino acid 386), LBR-ic4j (1815insGGAA, causing substitution of amino acids 606-627 and addition of 21 novel amino acids), and LBR-GT (β-geo gene trap in-frame insertion at amino acid 366).

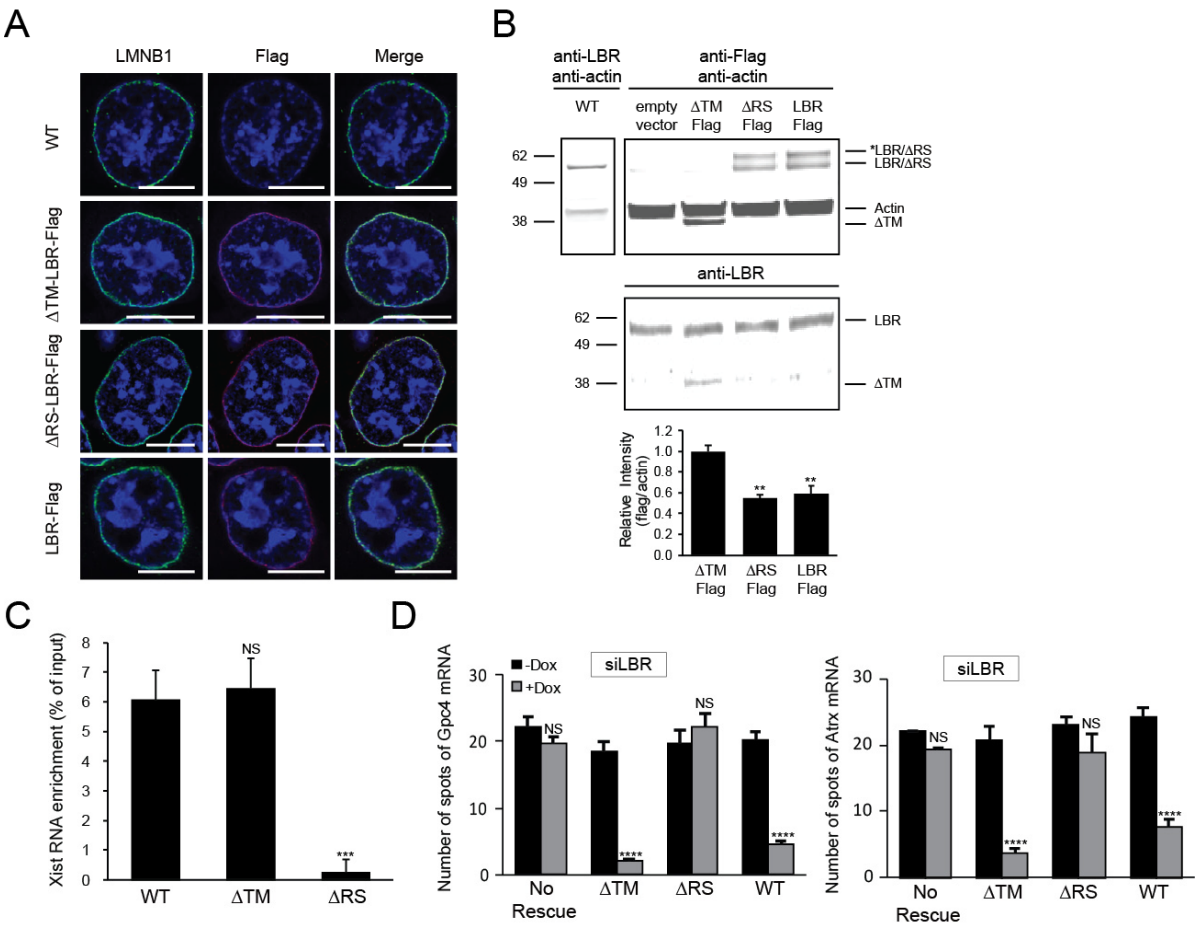

Fig. S6. ΔRS-LBR and ΔTM-LBR localize properly in the nuclear envelope, but ΔRS-LBR fails to rescue the Xist silencing defect upon knock down of endogenous LBR.

(A) Images of individual cell stained with endogenous LMNB1 (green) and FLAG-tag (red) in cells transfected with empty vector (WT) or λN-3xFLAG tagged ΔTM-LBR, ΔRS-LBR, or full-length LBR. The λN-3xFLAG tagged proteins colocalize with endogenous LMNB1 demonstrating that these mutants localize properly in the nuclear envelope. Scale bars: 5 micrometers. (B) Western blot using antibodies against FLAG-tag, endogenous LBR, and actin in cells transfected with empty vector or different λN-3xFLAG tagged ΔTM-LBR, ΔRS-LBR, or full-length LBR. Transfected cells express the tagged proteins at the anticipated size. The expression level of tagged proteins is plotted as the normalized level relative to the expression level of actin. *indicates a second LBR band that can be seen only when using a FLAG antibody, but not when using an endogenous LBR antibody in these same samples. Although it is unclear what this second band represents, it has been previously reported with certain endogenous antibodies and might reflect a phosphorylated form of LBR. Error bars represent the standard error from three independent Western blotting experiments. ** p-value<0.01 relative to ΔTM-LBR by an unpaired two-sample t-test. (C) Xist RNA levels measured by RT-qPCR after immunoprecipitation of a 3x-FLAG tagged LBR mutants relative to the input in cells expressing full-length LBR (WT), ΔRS-LBR, or ΔTM-LBR. Error bars represent the standard error from three independent IP experiments. NS: not significantly different

from the input; *** represents values significantly different from the input with a p-value<0.005 based on an unpaired two-sample t-test. (D) Quantification of the copy number of Gpc4 and Atrx mRNA prior to Xist induction (-Dox) and after Xist induction (+Dox) upon siRNA knockdown of the endogenous LBR and expression of empty vector (no rescue) or a cDNA construct expressing the ΔTM-LBR, ΔRS-LBR, or full length LBR (WT). NS: not significant, **** p-value<0.001 relative to –Dox cells by an unpaired two-sample t-test.

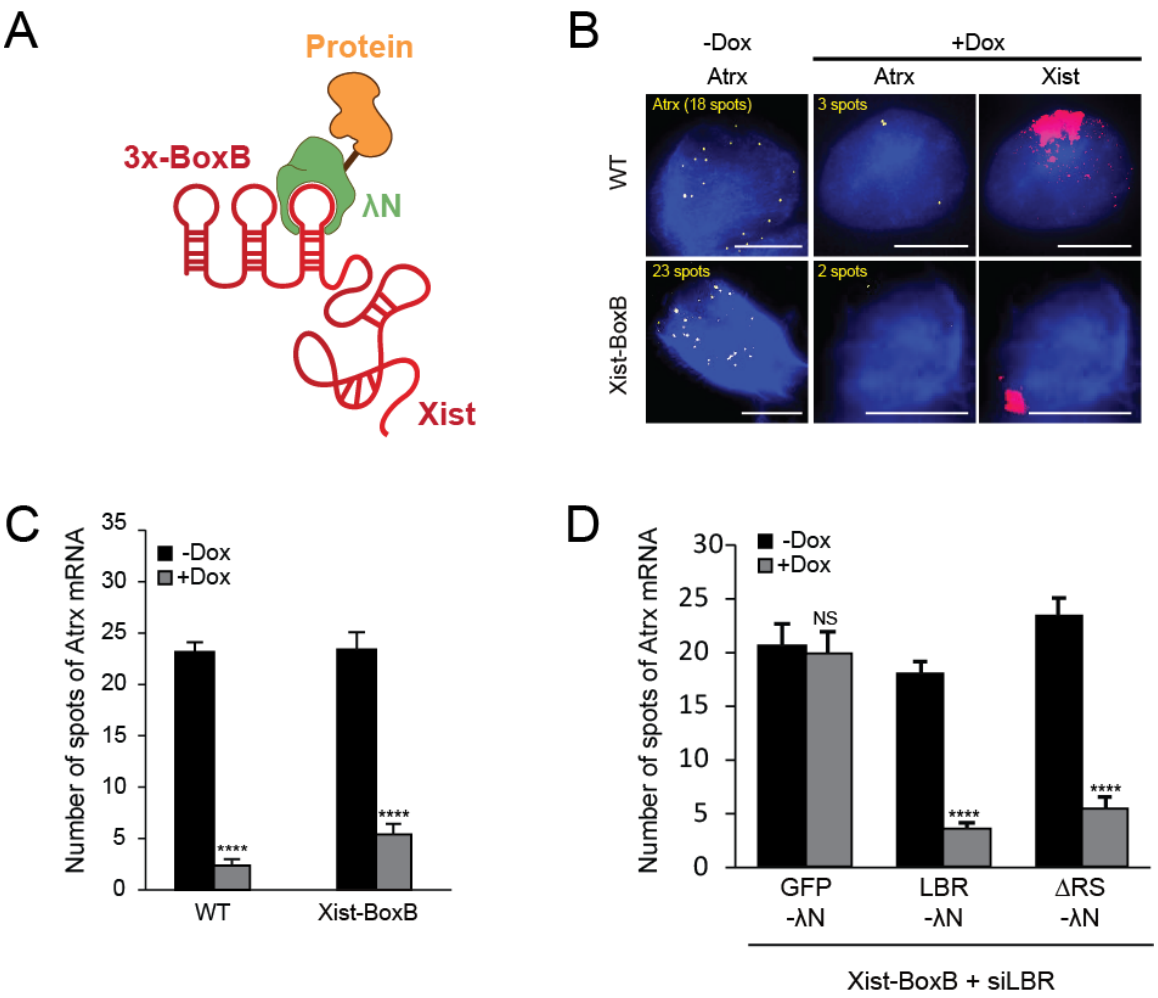

Fig. S7. The Xist-BoxB fusion RNA properly silences the X-chromosome.
(A) A schematic of the interaction between λN-fusion protein and Xist containing 3 copies of the BoxB RNA aptamer. (B) Images of individual cell for Atrx mRNA (yellow) along with Xist (red) and DAPI (blue) in cells expressing Xist fused with 3x-BoxB cells. The number of Atrx molecules is shown. Scale bars: 5 micrometers. (C) Quantification of the copy number of Atrx mRNA prior to Xist-BoxB induction (-Dox) and after Xist-BoxB induction (+Dox). Error bars represent the standard error across 50 individual cells. NS: not significant, **** p-value<0.001 relative to -Dox cells by an unpaired two-sample t-test. (D) Quantification of the copy number of Atrx mRNA prior to Xist induction (-Dox) and after Xist induction (+Dox) in Xist-BoxB cells after knockdown of the endogenous LBR and expression of GFP-λN (control), LBR-λN, or ΔRS-LBR-λN. NS: not significant, **** p-value<0.001 relative to –Dox cells by an unpaired two-sample t-test. Error bars represent the standard error across 50 individual cells.

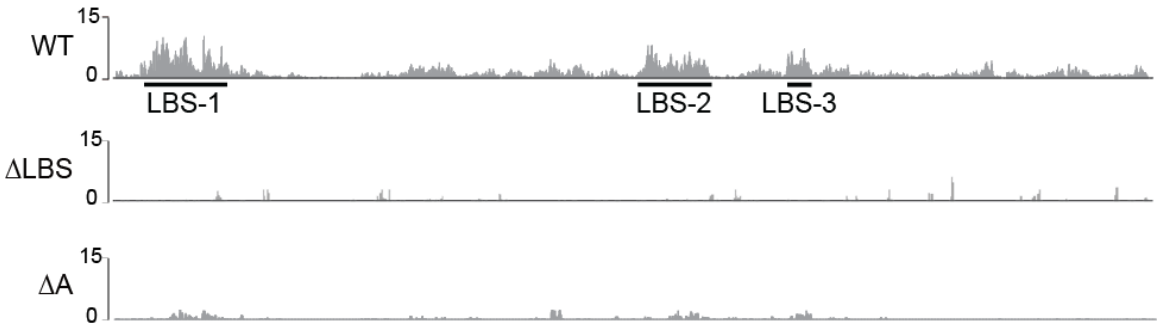

Fig. S8. Deletion of the A-repeat region or the LBS-1 region of Xist abolishes LBR binding across Xist.
CLIP result for LBR across the Xist RNA for wild type sample, ΔLBS, and ΔA cells. The values represent the fold-enrichment of each sample at each position on Xist RNA normalized to the input RNA from each sample. Note: The wild-type sample is the same as Figure 2A and is reproduced for ease of comparison.

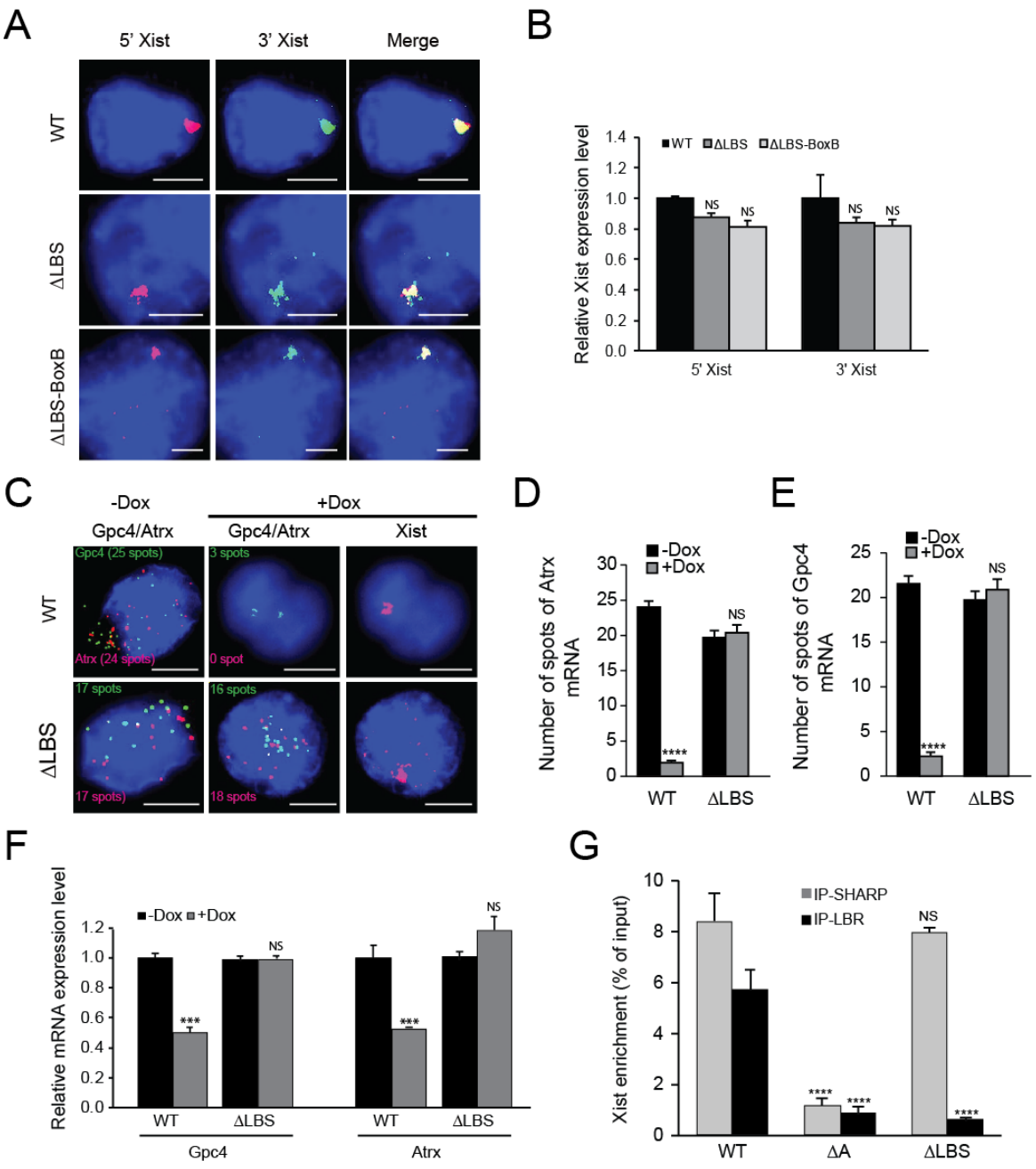

Fig. S9. Deletion of the LBR binding site on Xist ablates Xist-mediated silencing without impacting Xist RNA stability.

(A) RNA-FISH using probes against the 5' end of Xist (1285-2293; red) and the 3' end of Xist (10255-11912; green) in cells expressing wild-type Xist, ΔLBS-Xist, and ΔLBS-BoxB-Xist. The two sets of probes colocalize with each other, demonstrating that deletion of the LBR binding site on Xist does not affect the integrity of Xist RNA. (B) RT-qPCR of Xist using primers targeting 5' end of Xist (5104-5243) and 3' end of Xist (14117-14289) in cells expressing wild-type Xist (WT), ΔLBS-Xist, and ΔLBS-BoxB-Xist. Deletion of the LBR binding site on Xist does not affect the expression level of Xist relative to the wild-type. The Xist expression level is normalized to the expression level

of Gapdh RNA of each sample followed by a second normalization to the WT cells. Error bars represent the standard error from three independent RT-qPCR experiments. NS: not significant relative to WT cells by an unpaired two-sample t-test. (C) Images of individual cell for two X-linked mRNAs, Gpc4 (green) and Atrx (red) along with Xist (red) and DAPI (blue) in cells expressing ΔLBS-Xist. The number of identified mRNAs is shown. Scale bars: 5 micrometers. (D) and (E) Quantification of the copy number of Gpc4 and Atrx mRNA for –Dox and +Dox cells expressing ΔLBS-Xist. Error bars represent the standard error across 50 individual cells. NS: not significant, **** p-value<0.001 relative to –Dox cells by an unpaired two-sample t-test. (F) Gpc4 and Atrx RNA levels measured by RT-qPCR in cells expressing wild-type Xist (WT) or ΔLBS-Xist (ΔLBS) after Xist induction (+Dox) and prior to Xist induction (-Dox). The RNA expression level is normalized to the expression level of Gapdh RNA followed by a second normalization to the -Dox cells of each sample. Error bars represent the standard error across 4 independent experiments. NS: not significant, *** p-value<0.005 relative to -Dox cells by an unpaired two-sample t-test. (G) Xist RNA enrichment level measured by RT-qPCR after immunoprecipitation of endogenous LBR or SHARP in wild-type, ΔA, or ΔLBS cells relative to the input. Error bars: standard error from four independent IP experiments. NS: not significant, **** p-value<0.001 relative to wild type cells.

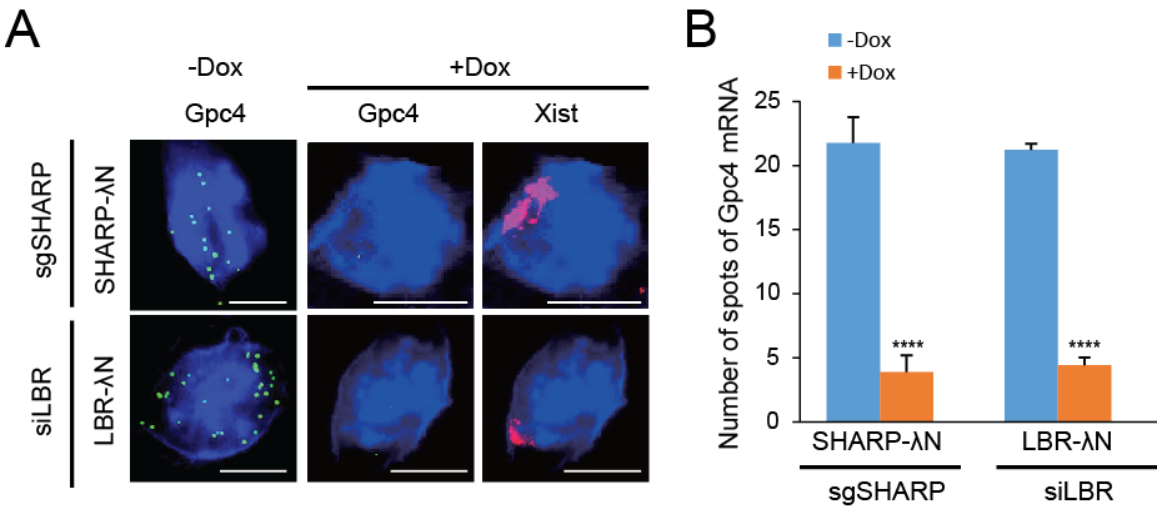

Fig. S10. λN-3xFLAG tagged LBR and SHARP are functional proteins that can compensate for the endogenous protein in Xist-mediated silencing.
(A) Images of individual cell for Gpc4 mRNAs (green) and Xist (red) along with DAPI (blue) in cells expressing SHARP- λN-3xFLAG or LBR- λN-3xFLAG upon knock down of SHARP using CRISPRi or knock down of LBR using siRNAs. Scale bars: 5 micrometers. (B) Quantification of the copy number of Gpc4 mRNA for -Dox and +Dox cells expressing SHARP- λN-3xFLAG or LBR- λN-3xFLAG upon knock down of SHARP or LBR. Error bars represent the standard error across 50 individual cells. **** p-value<0.001 relative to -Dox cells by an unpaired two-sample t-test.

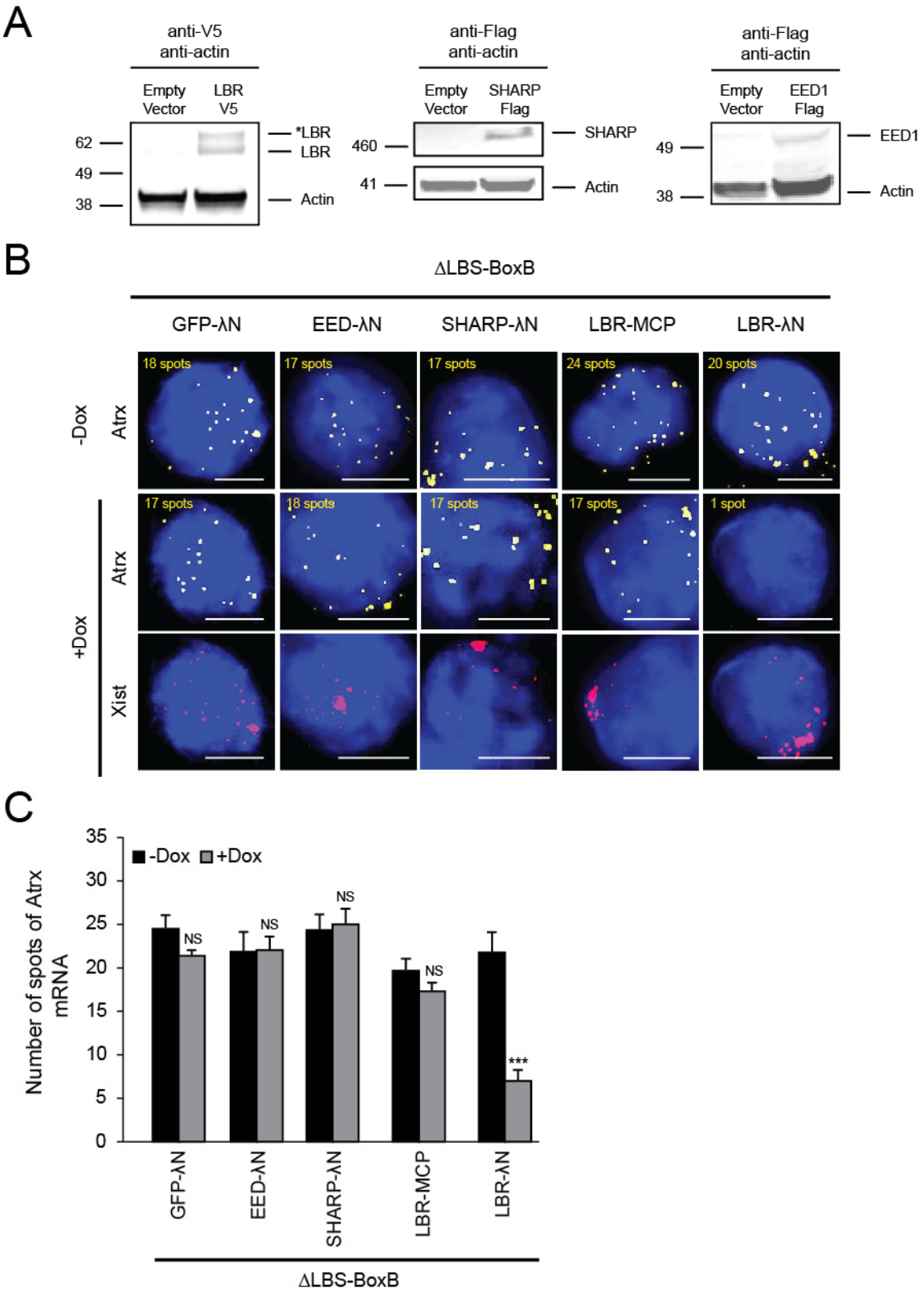

Fig. S11. Tethering LBR-λN to ΔLBS-Xist rescues the Xist silencing defect in ΔLBS cells.

(A) Western blot using antibodies against FLAG-tag, V5-tag, and actin of cells transfected with empty vector, MCP-V5 tagged LBR, or λN-3xFLAG tagged SHARP or EED1. Transfected cells can express the tagged proteins of the anticipated size. * indicates the possible phosphorylated form of LBR. (B) Images of individual cell for Atrx mRNA (yellow) and Xist (red) along with DAPI (blue) in cells expressing ΔLBS-BoxB Xist after transfecting with different fusion proteins. The number of identified mRNAs is shown. Scale bars: 5 micrometers. (C) Quantification of the copy number of Atrx mRNA for -Dox and +Dox cells expressing ΔLBS-BoxB Xist after transfecting with different fusion proteins. Error bars represent the standard error across 50 individual cells. NS: not significant, *** p-value<0.005 relative to -Dox cells by an unpaired two-sample t-test.

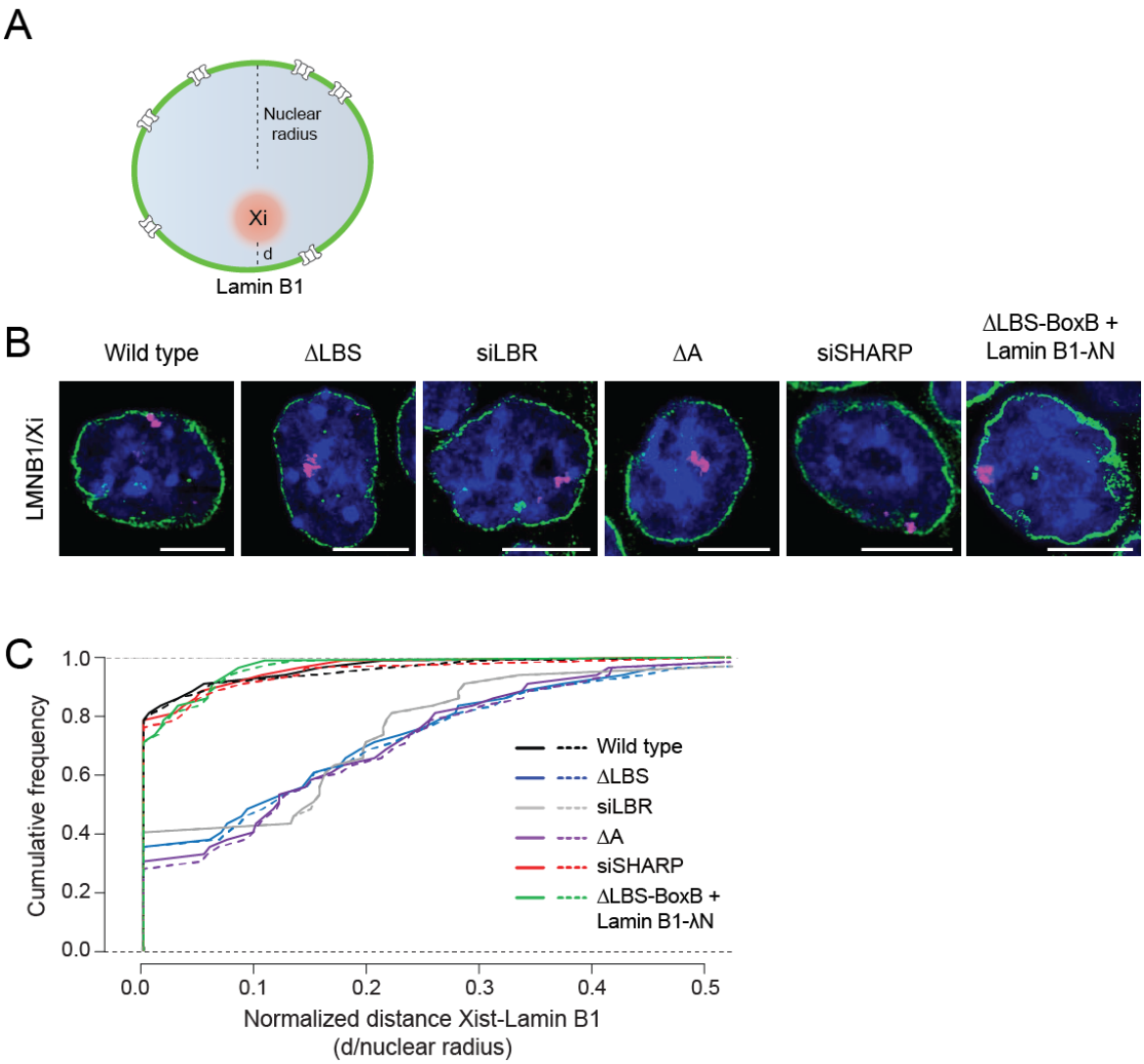

Fig. S12. Xist-mediated recruitment of inactive X-chromosome to the nuclear lamina is dependent on LBR.

(A) A schematic illustrating the normalized distance calculation between the X chromosome and Lamin B1. (B) Images of individual cells where the X chromosome is labeled by chromosome paint (red) along with immunofluorescence for Lamin B1 protein (green) and DAPI (blue) across different conditions. Scale bars: 5 micrometers. (C) The cumulative frequency distribution of normalized distances between the X chromosome and Lamin B1 across 40 individual cells. Dashed lines represents a second independent chromosome paint experiment.

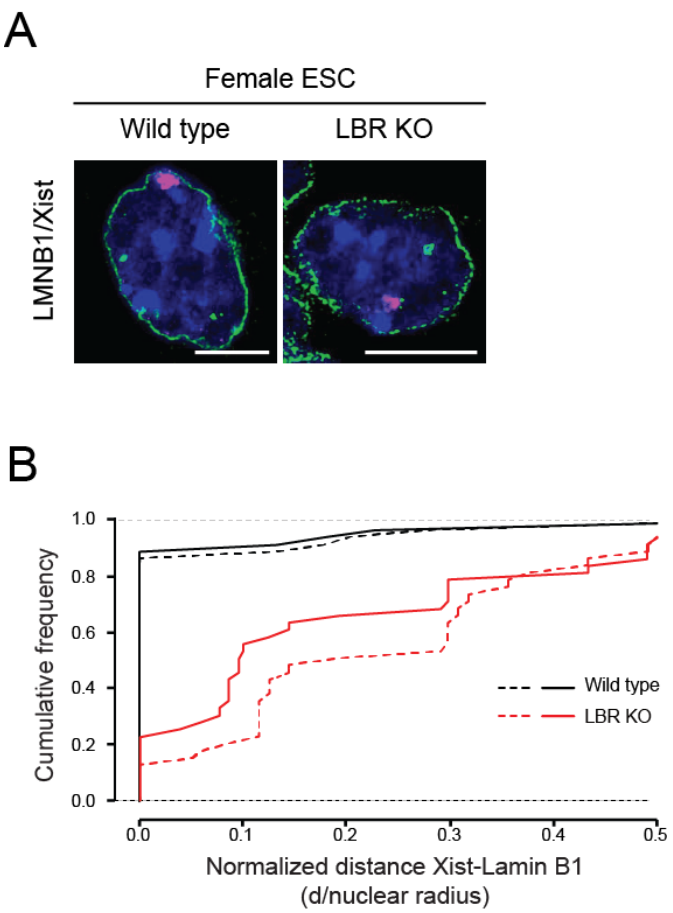

Fig. S13. Xist-mediated recruitment to the nuclear lamina is dependent on LBR in differentiating female ES cells.
(A) Images of individual female ES cell that are labeled with Xist (red), Lamin B1 (green) and DAPI (blue) in wild-type or LBR knockout female ES cells. Scale bars: 5 micrometers. (B) The cumulative frequency distribution of normalized distances between Xist and Lamin B1 across 40 individual cells from two independent IF/FISH experiments. Dashed lines represents a second independent experiment.

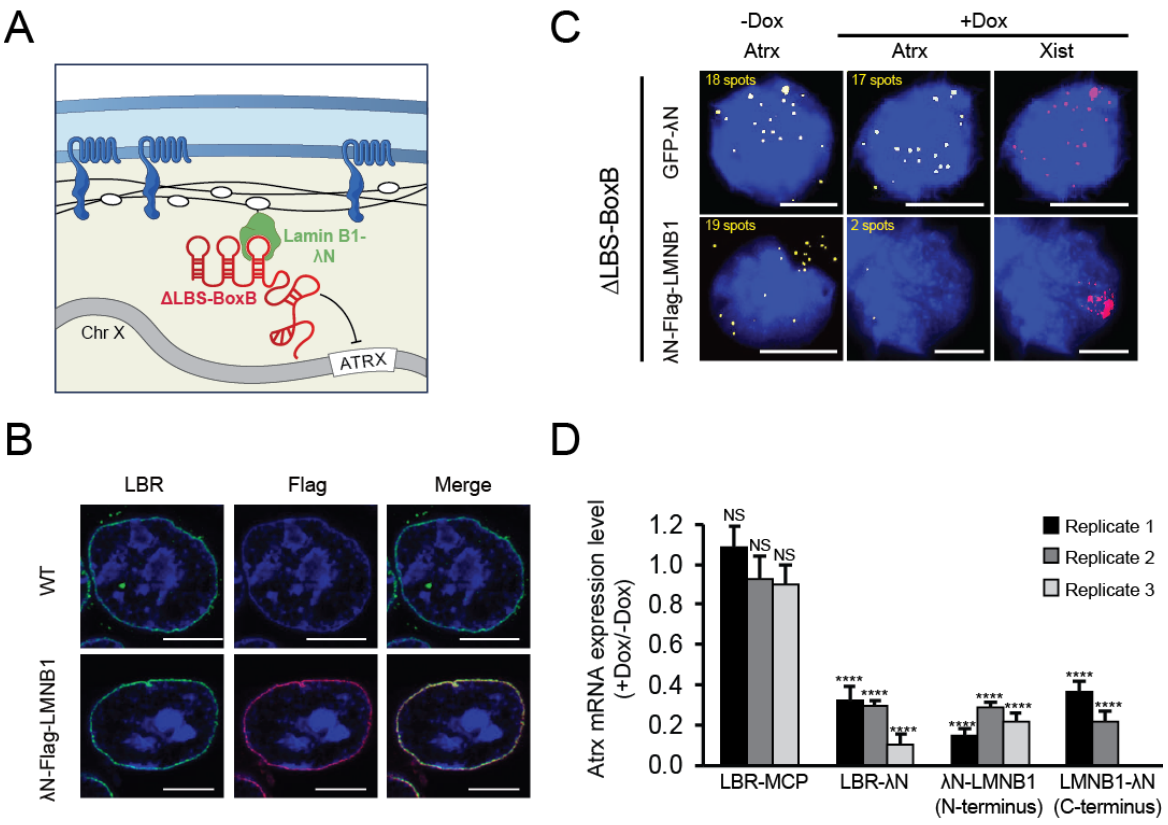

Fig. S14. Recruiting ΔLBS Xist to the nuclear lamina rescues the Xist silencing defect.

(A) A schematic illustrating the tethering of ΔLBS-BoxB to the nuclear lamina using the LaminB1-λN fusion protein. (B) Images of individual cell stained with endogenous LBR (green) and FLAG-tag (red) in cells transfected with empty vector (WT) or λN-3xFLAG tagged LMNB1. The λN-3xFLAG tagged LMNB1 localizes properly in the nuclear envelope and colocalize with endogenous LBR. Scale bars: 5 micrometers. (C) Images of individual cells for Atrx mRNAs (yellow) and Xist (red) along with DAPI (blue) in cells expressing ΔLBS-BoxB Xist transfected with λN-LMNB1 fusion protein. The number of identified mRNAs is shown. Scale bars: 5 micrometers. (D) Three independent replicates (two for LMNB1-λN) showing the copy number of Atrx mRNA molecules after induction of Xist normalized to the number of the mRNA molecules prior to Xist induction in cells expressing ΔLBS-BoxB Xist transfecting with LBR-MCP, LBR-λN, λN-LMNB1 or LMNB1-λN fusion protein. Error bars represent the standard error across 50 individual cells. NS: not significantly different from 1; **** represents values significantly different from 1 with a p-value<0.0001 based on a one-sample t-test.

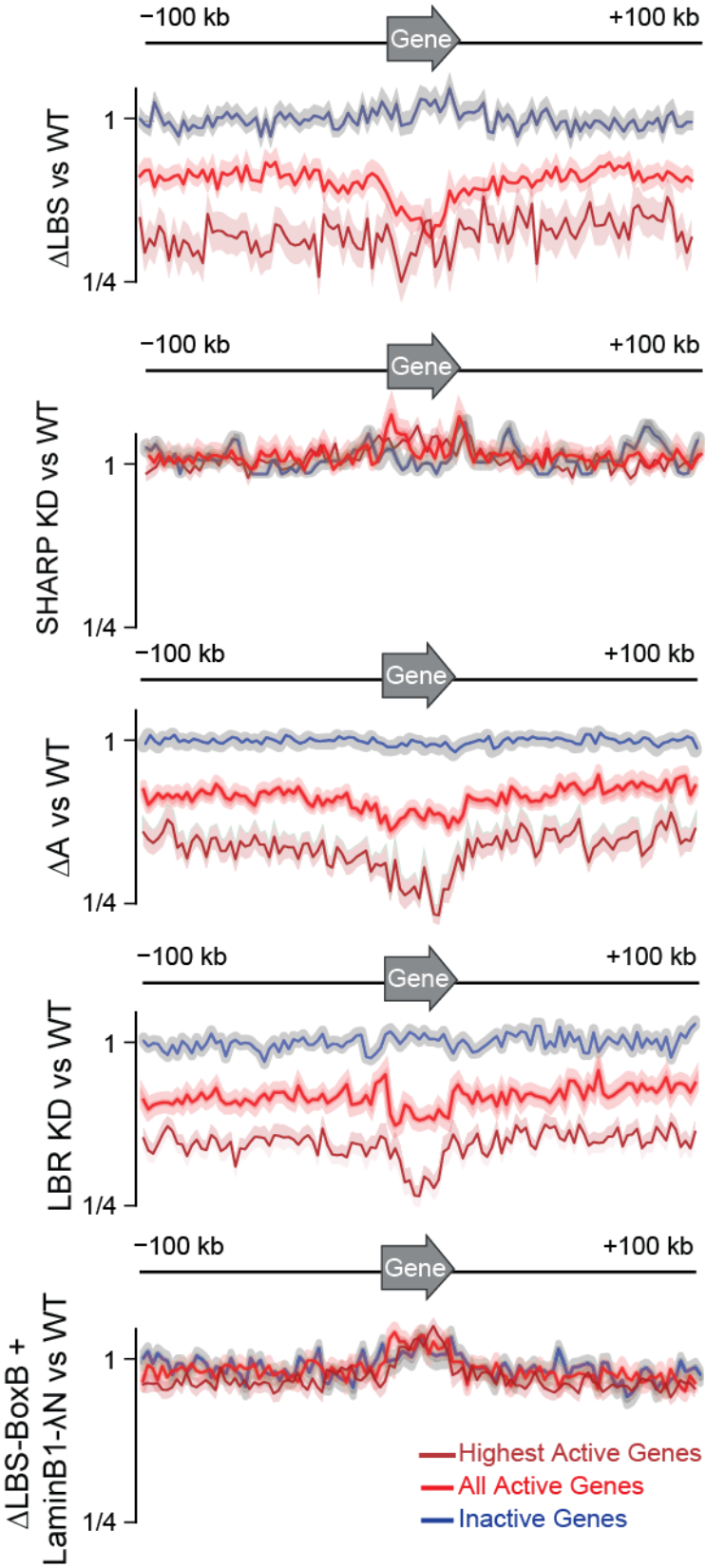
−100 kb
Gene
+100 kb
ΔLBS vs WT
1
1/4
SHARP KD vs WT
ΔA vs WT
LBR KD vs WT
ΔLBS-BoxB +
LaminB1-λN vs WT
Highest Active Genes
All Active Genes
Inactive Genes

Fig. S15. ΔLBS-Xist fails to spread to active genes, but this defect can be rescued by synthetically recruiting ΔLBS-Xist to the nuclear lamina.
Fold-change of Xist enrichment across the X chromosome as measured by RAP-DNA averaged across the most highly actively transcribed genes (dark red, RPKM expression >5), all actively transcribed genes (red, RPKM >1), and inactive genes (blue) on the X-chromosome for ΔLBS, SHARP knock down, ΔA, LBR knockdown, and ΔLBS-BoxB + LMNB1-λN cells in comparison to wild type Xist cells. Shaded areas represent 95% confidence interval for the average enrichment. Enrichment level are normalized to the mean across the X-chromosome and are plotted on a log scale. Same panels from Fig. 4B were used for comparison.

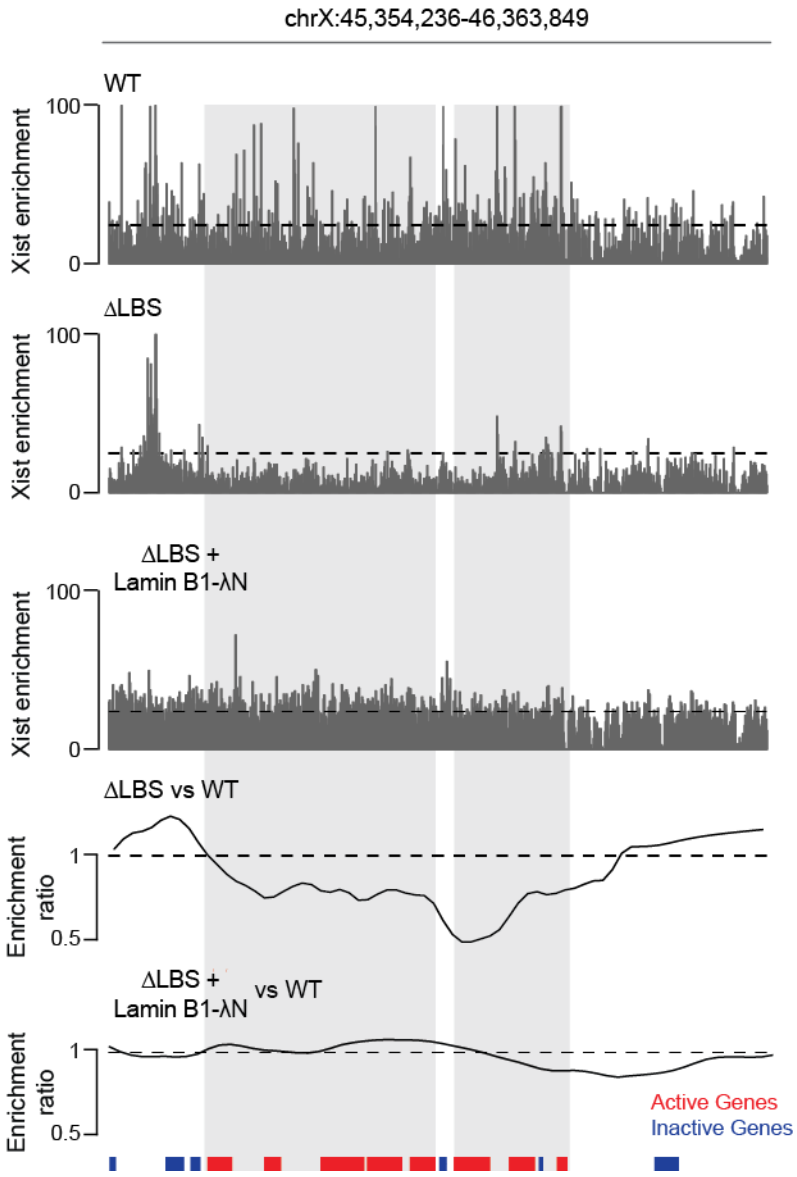

Fig. S16. Recruiting Xist to the nuclear lamina allows Xist to spread to actively transcribed genes on X-chromosome.
Xist RNA localization as measured by RAP-DNA for wild type, ΔLBS-Xist, and LMNB1-λN in ΔLBS-BoxB cells and the smoothed fold change across a region of the X chromosome containing active (red) and inactive (blue) genes. Dashed line: average Xist enrichment in wild type cells. Same panels from Fig. 4A were used for comparison.

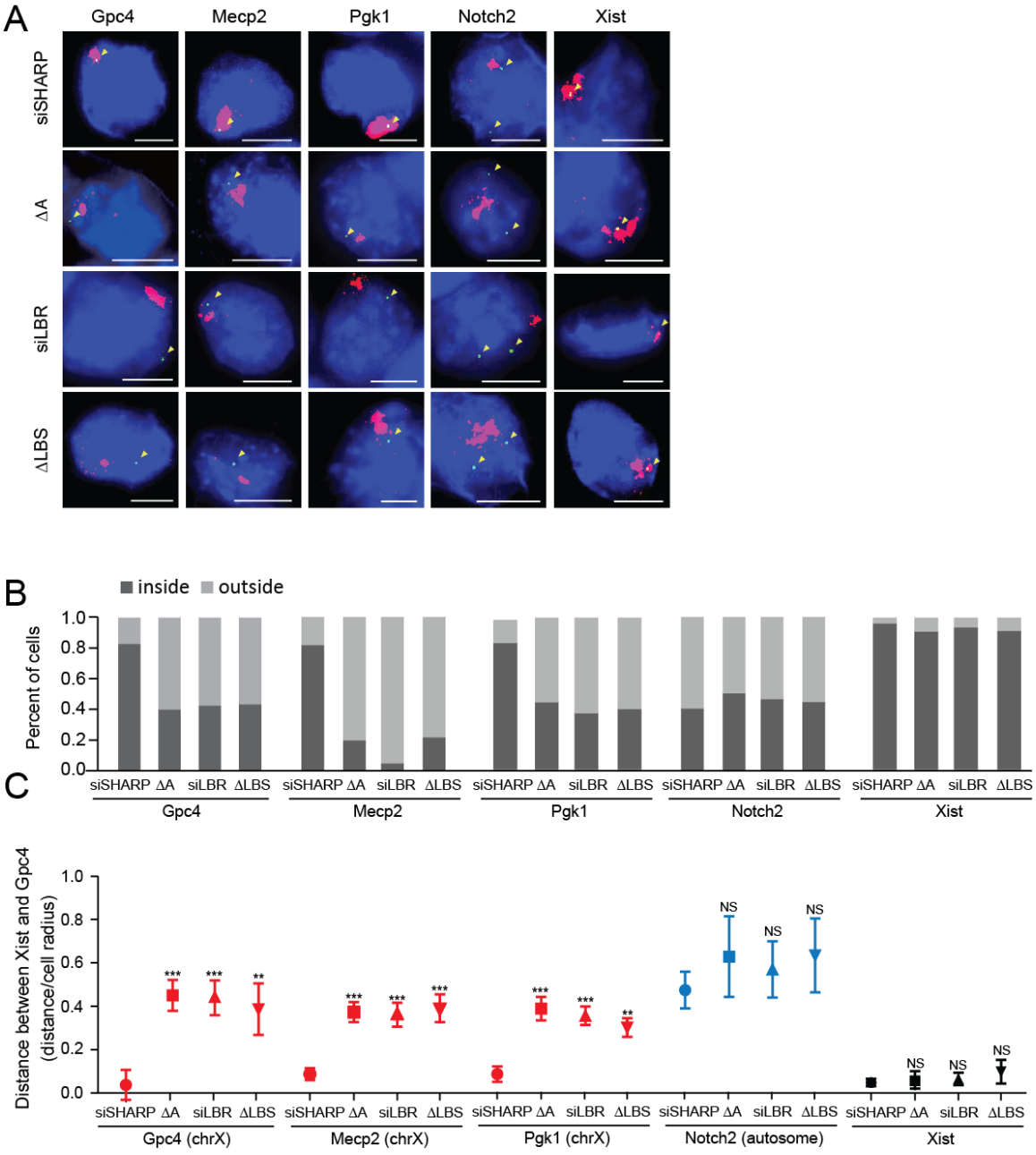

Fig. S17. Recruitment to the nuclear lamina is required for repositioning active genes into the Xist-coated nuclear compartment.
(A) Images of individual cell that are labeled with Gpc4, Mecp2, Pgk1 locus, Notch2 loci, or Xist genomic locus (green) along with Xist RNA (red) and DAPI (blue) across different cell lines (rows). (B) The percentage of cells where the Gpc4, Mecp2, Pgk1 locus, Notch2 loci or Xist locus were found inside or outside of the Xist compartment across 80 cells. (C) The median distance from the Gpc4, Mecp2, Pgk1 locus, Notch2 loci or Xist locus to the Xist compartment across different conditions. Error bars represent the standard error of the median across 80 individual cells. NS: not significant, ** p-value<0.01, *** p-value<0.005 relative to siSHARP by an unpaired two-sample t-test.

Scale bars: 5 micrometers. Note: The Gpc4, Mecp2 and Pgk1 graphs are the same as those shown in Figure 4E and are included for ease of comparison.

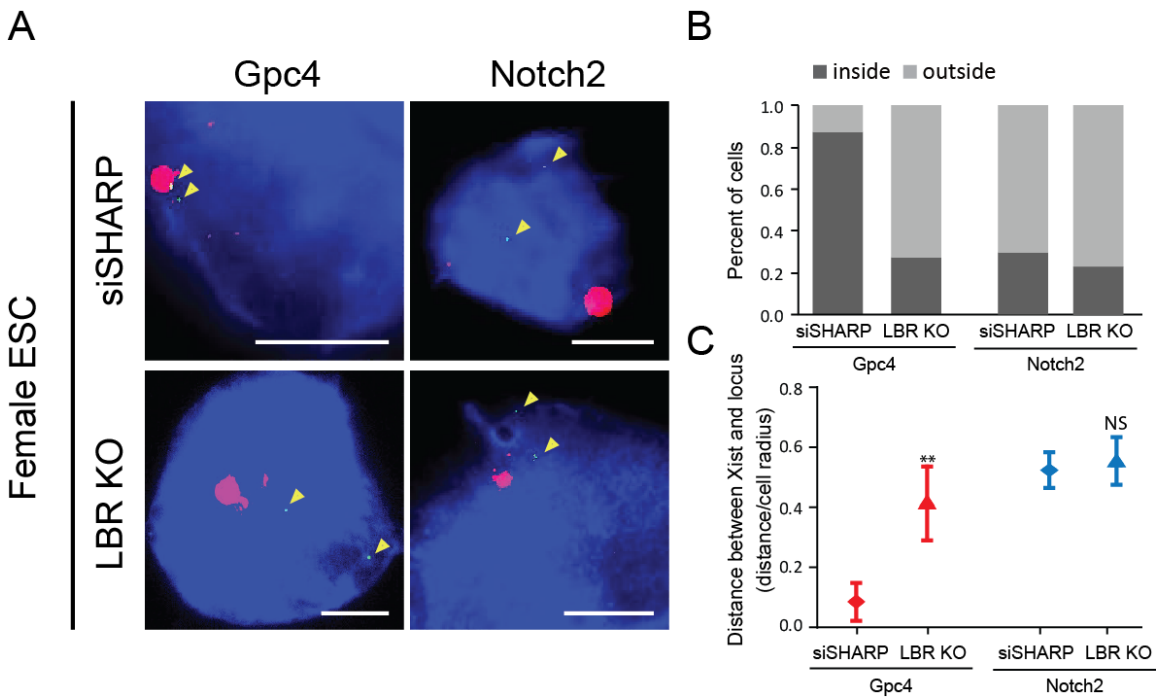

Fig. S18. Recruitment to the nuclear lamina is required for repositioning active genes into the Xist-coated nuclear compartment in female ES cells.
(A) Images of individual cell that are labeled with the Gpc4 loci or Notch2 loci (green) along with Xist RNA (red) and DAPI (blue) in SHARP knockdown and LBR knockout female ES cells (B) The percentage of cells where the Gpc4 loci or Notch2 loci were found inside or outside of the Xist cloud across 80 cells. (C) The median distance from Gpc4 loci or Notch2 loci to Xist cloud across different cell lines across 80 cells. Error bars represent the standard error of the median across 80 individual cells. NS: not significant, ** p-value<0.01 relative to siSHARP by an unpaired two-sample t-test. Scale bars: 5 micrometers.

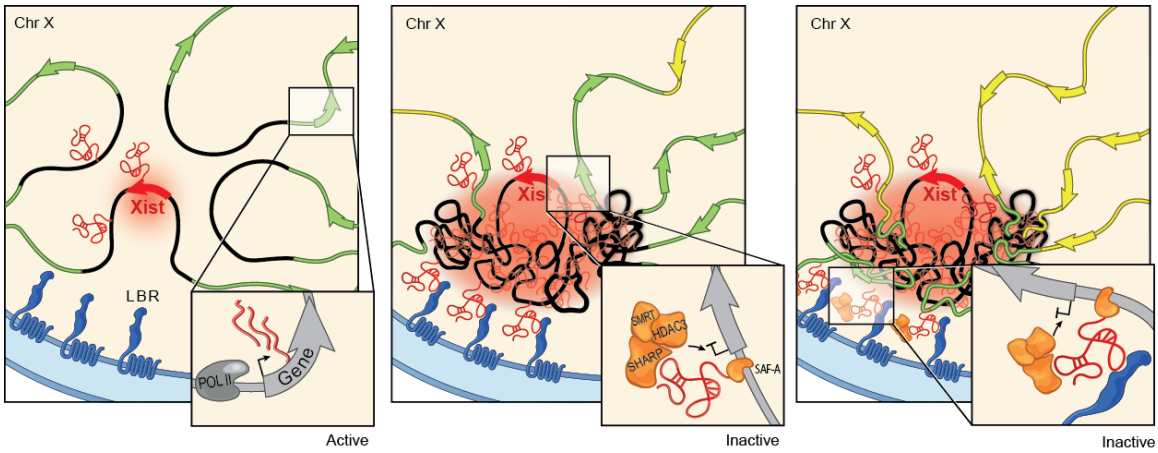

Fig. S19. A model for how Xist-mediated recruitment to the nuclear lamina enables spreading to active genes and transcriptional silencing on the X chromosome. Our results demonstrate that recruitment of the X chromosome to the nuclear lamina is required for Xist RNA spreading to actively transcribed genes on the X chromosome and that this spreading enables Xist to silence transcription through SHARP. We propose a model to explain how these structural changes allow Xist to spread to actively transcribed genes by incorporating our observations with previous observations about Xist RNA spreading and chromosome dynamics. Upon initiation (left panel), Xist spreads to regions that are closest to the Xist transcription locus (red arrow) (*7*, *8*), which are generally depleted for actively transcribed genes (*7*, *8*, *6*, *9*). These initial Xist-coated DNA regions (black regions) sample different locations of the nucleus (*44*, *45*, *23*, *46*, *47*) and when they come into close proximity of the nuclear lamina, are sequestered at the nuclear lamina through an interaction between Xist and LBR (middle panel). Because DNA that interacts with the nuclear lamina undergoes more constrained mobility (*23*, *24*), this recruitment changes the 3-dimensional organization of X-chromosome (*15*, *48*, *49*) and repositions active genes (green regions) closer the Xist transcription locus enabling Xist, and its SHARP/SMRT/HDAC3 silencing complex (*11*, *18*, *22*), to spread to these new sites by 3-dimensional proximity transfer. These sites are then recruited to the nuclear lamina, effectively bringing another set of active genes (yellow regions) into closer contact with the Xist transcription locus (right panel). Because the Xist transcription locus escapes Xist coating and silencing, it is positioned away from the nuclear lamina (*7*, *8*, *5*, *2*, *1*) and therefore will be close to sites that have not yet been coated and silenced by Xist. This iterative process would enable Xist to spread to, and silence, actively transcribed genes across the entire X-chromosome.

References and Notes

1. R. Galupa, E. Heard, X-chromosome inactivation: New insights into cis and trans regulation. *Curr. Opin. Genet. Dev.* **31**, 57–66 (2015). Medline doi:10.1016/j.gde.2015.04.002

2. E. Splinter, E. de Wit, E. P. Nora, P. Klous, H. J. van de Werken, Y. Zhu, L. J. Kaaij, W. van Ijcken, J. Gribnau, E. Heard, W. de Laat, The inactive X chromosome adopts a unique three-dimensional conformation that is dependent on Xist RNA. *Genes Dev.* **25**, 1371–1383 (2011). Medline doi:10.1101/gad.633311

3. S. S. Rao, M. H. Huntley, N. C. Durand, E. K. Stamenova, I. D. Bochkov, J. T. Robinson, A. L. Sanborn, I. Machol, A. D. Omer, E. S. Lander, E. L. Aiden, A 3D map of the human genome at kilobase resolution reveals principles of chromatin looping. *Cell* **159**, 1665–1680 (2014). Medline doi:10.1016/j.cell.2014.11.021

4. A. Rego, P. B. Sinclair, W. Tao, I. Kireev, A. S. Belmont, The facultative heterochromatin of the inactive X chromosome has a distinctive condensed ultrastructure. *J. Cell Sci.* **121**, 1119–1127 (2008). Medline doi:10.1242/jcs.026104

5. A. Wutz, Gene silencing in X-chromosome inactivation: Advances in understanding facultative heterochromatin formation. *Nat. Rev. Genet.* **12**, 542–553 (2011). Medline doi:10.1038/nrg3035

6. C. M. Clemson, L. L. Hall, M. Byron, J. McNeil, J. B. Lawrence, The X chromosome is organized into a gene-rich outer rim and an internal core containing silenced nongenic sequences. *Proc. Natl. Acad. Sci. U.S.A.* **103**, 7688–7693 (2006). Medline doi:10.1073/pnas.0601069103

7. J. M. Engreitz, A. Pandya-Jones, P. McDonel, A. Shishkin, K. Sirokman, C. Surka, S. Kadri, J. Xing, A. Goren, E. S. Lander, K. Plath, M. Guttman, The Xist lncRNA exploits three-dimensional genome architecture to spread across the X chromosome. *Science* **341**, 1237973 (2013). Medline doi:10.1126/science.1237973

8. M. D. Simon, S. F. Pinter, R. Fang, K. Sarma, M. Rutenberg-Schoenberg, S. K. Bowman, B. A. Kesner, V. K. Maier, R. E. Kingston, J. T. Lee, High-resolution Xist binding maps reveal two-step spreading during X-chromosome inactivation. *Nature* **504**, 465–469 (2013). Medline doi:10.1038/nature12719

9. J. Chaumeil, P. Le Baccon, A. Wutz, E. Heard, A novel role for Xist RNA in the formation of a repressive nuclear compartment into which genes are recruited when silenced. *Genes Dev.* **20**, 2223–2237 (2006). Medline doi:10.1101/gad.380906

10. A. Wutz, T. P. Rasmussen, R. Jaenisch, Chromosomal silencing and localization are mediated by different domains of Xist RNA. *Nat. Genet.* **30**, 167–174 (2002). Medline doi:10.1038/ng820

11. C. A. McHugh, C. K. Chen, A. Chow, C. F. Surka, C. Tran, P. McDonel, A. Pandya-Jones, M. Blanco, C. Burghard, A. Moradian, M. J. Sweredoski, A. A. Shishkin, J. Su, E. S. Lander, S. Hess, K. Plath, M. Guttman, The Xist lncRNA interacts

directly with SHARP to silence transcription through HDAC3. *Nature* **521**, 232–236 (2015). Medline doi:10.1038/nature14443

12. C. Chu, Q. C. Zhang, S. T. da Rocha, R. A. Flynn, M. Bharadwaj, J. M. Calabrese, T. Magnuson, E. Heard, H. Y. Chang, Systematic discovery of Xist RNA binding proteins. *Cell* **161**, 404–416 (2015). Medline doi:10.1016/j.cell.2015.03.025

13. A. Minajigi, J. E. Froberg, C. Wei, H. Sunwoo, B. Kesner, D. Colognori, D. Lessing, B. Payer, M. Boukhali, W. Haas, J. T. Lee, A comprehensive Xist interactome reveals cohesin repulsion and an RNA-directed chromosome conformation. *Science* **349**, aab2276 (2015). Medline doi:10.1126/science.aab2276

14. Y. Gruenbaum, A. Margalit, R. D. Goldman, D. K. Shumaker, K. L. Wilson, The nuclear lamina comes of age. *Nat. Rev. Mol. Cell Biol.* **6**, 21–31 (2005). Medline doi:10.1038/nrm1550

15. A. Pombo, N. Dillon, Three-dimensional genome architecture: Players and mechanisms. *Nat. Rev. Mol. Cell Biol.* **16**, 245–257 (2015). Medline doi:10.1038/nrm3965

16. J. Kind, B. van Steensel, Genome-nuclear lamina interactions and gene regulation. *Curr. Opin. Cell Biol.* **22**, 320–325 (2010). Medline doi:10.1016/j.ceb.2010.04.002

17. J. Baron-Benhamou, N. H. Gehring, A. E. Kulozik, M. W. Hentze, Using the lambdaN peptide to tether proteins to RNAs. *Methods Mol. Biol.* **257**, 135–154 (2004). Medline

18. A. Monfort, G. Di Minin, A. Postlmayr, R. Freimann, F. Arieti, S. Thore, A. Wutz, Identification of *Spen* as a Crucial Factor for *Xist* Function through Forward Genetic Screening in Haploid Embryonic Stem Cells. *Cell Rep.* **12**, 554–561 (2015). Medline doi:10.1016/j.celrep.2015.06.067

19. A. R. Buxbaum, G. Haimovich, R. H. Singer, In the right place at the right time: Visualizing and understanding mRNA localization. *Nat. Rev. Mol. Cell Biol.* **16**, 95–109 (2015). Medline doi:10.1038/nrm3918

20. L. E. Finlan, D. Sproul, I. Thomson, S. Boyle, E. Kerr, P. Perry, B. Ylstra, J. R. Chubb, W. A. Bickmore, Recruitment to the nuclear periphery can alter expression of genes in human cells. *PLoS Genet.* **4**, e1000039 (2008). Medline doi:10.1371/journal.pgen.1000039

21. K. L. Reddy, J. M. Zullo, E. Bertolino, H. Singh, Transcriptional repression mediated by repositioning of genes to the nuclear lamina. *Nature* **452**, 243–247 (2008). Medline doi:10.1038/nature06727

22. B. Moindrot, A. Cerase, H. Coker, O. Masui, A. Grijzenhout, G. Pintacuda, L. Schermelleh, T. B. Nesterova, N. Brockdorff, A Pooled shRNA Screen Identifies Rbm15, Spen, and Wtap as Factors Required for Xist RNA-Mediated Silencing. *Cell Rep.* **12**, 562–572 (2015). Medline doi:10.1016/j.celrep.2015.06.053

23. W. F. Marshall, A. Straight, J. F. Marko, J. Swedlow, A. Dernburg, A. Belmont, A. W. Murray, D. A. Agard, J. W. Sedat, Interphase chromosomes undergo

constrained diffusional motion in living cells. *Curr. Biol.* **7**, 930–939 (1997). Medline doi:10.1016/S0960-9822(06)00412-X

24. J. R. Chubb, S. Boyle, P. Perry, W. A. Bickmore, Chromatin motion is constrained by association with nuclear compartments in human cells. *Curr. Biol.* **12**, 439–445 (2002). Medline doi:10.1016/S0960-9822(02)00695-4

25. A. A. Shishkin, G. Giannoukos, A. Kucukural, D. Ciulla, M. Busby, C. Surka, J. Chen, R. P. Bhattacharyya, R. F. Rudy, M. M. Patel, N. Novod, D. T. Hung, A. Gnirke, M. Garber, M. Guttman, J. Livny, Simultaneous generation of many RNA-seq libraries in a single reaction. *Nat. Methods* **12**, 323–325 (2015). Medline doi:10.1038/nmeth.3313

26. J. M. Engreitz, K. Sirokman, P. McDonel, A. A. Shishkin, C. Surka, P. Russell, S. R. Grossman, A. Y. Chow, M. Guttman, E. S. Lander, RNA-RNA interactions enable specific targeting of noncoding RNAs to nascent Pre-mRNAs and chromatin sites. *Cell* **159**, 188–199 (2014). Medline doi:10.1016/j.cell.2014.08.018

27. Z. Theodosiou, I. N. Kasampalidis, G. Livanos, M. Zervakis, I. Pitas, K. Lyroudia, Automated analysis of FISH and immunohistochemistry images: A review. *Cytometry A* **71**, 439–450 (2007). Medline doi:10.1002/cyto.a.20409

28. M. Fumagalli, F. Rossiello, M. Clerici, S. Barozzi, D. Cittaro, J. M. Kaplunov, G. Bucci, M. Dobreva, V. Matti, C. M. Beausejour, U. Herbig, M. P. Longhese, F. d'Adda di Fagagna, Telomeric DNA damage is irreparable and causes persistent DNA-damage-response activation. *Nat. Cell Biol.* **14**, 355–365 (2012). Medline doi:10.1038/ncb2466

29. M. J. Levesque, A. Raj, Single-chromosome transcriptional profiling reveals chromosomal gene expression regulation. *Nat. Methods* **10**, 246–248 (2013). Medline doi:10.1038/nmeth.2372

30. A. Wutz, R. Jaenisch, A shift from reversible to irreversible X inactivation is triggered during ES cell differentiation. *Mol. Cell* **5**, 695–705 (2000). Medline doi:10.1016/S1097-2765(00)80248-8

31. H. Shen, M. R. Green, A pathway of sequential arginine-serine-rich domain-splicing signal interactions during mammalian spliceosome assembly. *Mol. Cell* **16**, 363–373 (2004). Medline doi:10.1016/j.molcel.2004.10.021

32. J. Valcárcel, M. R. Green, The SR protein family: Pleiotropic functions in pre-mRNA splicing. *Trends Biochem. Sci.* **21**, 296–301 (1996). Medline doi:10.1016/S0968-0004(96)10039-6

33. O. A. Kent, A. Reayi, L. Foong, K. A. Chilibeck, A. M. MacMillan, Structuring of the 3′ splice site by U2AF65. *J. Biol. Chem.* **278**, 50572–50577 (2003). Medline doi:10.1074/jbc.M307976200

34. A. Castello, B. Fischer, K. Eichelbaum, R. Horos, B. M. Beckmann, C. Strein, N. E. Davey, D. T. Humphreys, T. Preiss, L. M. Steinmetz, J. Krijgsveld, M. W. Hentze, Insights into RNA biology from an atlas of mammalian mRNA-binding proteins. *Cell* **149**, 1393–1406 (2012). Medline doi:10.1016/j.cell.2012.04.031

35. E. Nikolakaki, V. Drosou, I. Sanidas, P. Peidis, T. Papamarcaki, L. M. Iakoucheva, T. Giannakouros, RNA association or phosphorylation of the RS domain prevents aggregation of RS domain-containing proteins. *Biochim. Biophys. Acta* **1780**, 214–225 (2008). Medline doi:10.1016/j.bbagen.2007.10.014

36. L. D. Shultz, B. L. Lyons, L. M. Burzenski, B. Gott, R. Samuels, P. A. Schweitzer, C. Dreger, H. Herrmann, V. Kalscheuer, A. L. Olins, D. E. Olins, K. Sperling, K. Hoffmann, Mutations at the mouse ichthyosis locus are within the lamin B receptor gene: A single gene model for human Pelger-Huët anomaly. *Hum. Mol. Genet.* **12**, 61–69 (2003). Medline doi:10.1093/hmg/ddg003

37. T. V. Cohen, K. D. Klarmann, K. Sakchaisri, J. P. Cooper, D. Kuhns, M. Anver, P. F. Johnson, S. C. Williams, J. R. Keller, C. L. Stewart, The lamin B receptor under transcriptional control of C/EBPepsilon is required for morphological but not functional maturation of neutrophils. *Hum. Mol. Genet.* **17**, 2921–2933 (2008). Medline doi:10.1093/hmg/ddn191

38. J. König, K. Zarnack, G. Rot, T. Curk, M. Kayikci, B. Zupan, D. J. Turner, N. M. Luscombe, J. Ule, iCLIP reveals the function of hnRNP particles in splicing at individual nucleotide resolution. *Nat. Struct. Mol. Biol.* **17**, 909–915 (2010). Medline doi:10.1038/nsmb.1838

39. D. D. Licatalosi, A. Mele, J. J. Fak, J. Ule, M. Kayikci, S. W. Chi, T. A. Clark, A. C. Schweitzer, J. E. Blume, X. Wang, J. C. Darnell, R. B. Darnell, HITS-CLIP yields genome-wide insights into brain alternative RNA processing. *Nature* **456**, 464–469 (2008). Medline doi:10.1038/nature07488

40. J. Ule, K. B. Jensen, M. Ruggiu, A. Mele, A. Ule, R. B. Darnell, CLIP identifies Nova-regulated RNA networks in the brain. *Science* **302**, 1212–1215 (2003). Medline doi:10.1126/science.1090095

41. A. S. Belmont, F. Bignone, P. O. Ts'o, The relative intranuclear positions of Barr bodies in XXX non-transformed human fibroblasts. *Exp. Cell Res.* **165**, 165–179 (1986). Medline doi:10.1016/0014-4827(86)90541-0

42. C. L. Walker, C. B. Cargile, K. M. Floy, M. Delannoy, B. R. Migeon, The Barr body is a looped X chromosome formed by telomere association. *Proc. Natl. Acad. Sci. U.S.A.* **88**, 6191–6195 (1991). Medline doi:10.1073/pnas.88.14.6191

43. L.-F. Zhang, K. D. Huynh, J. T. Lee, Perinucleolar targeting of the inactive X during S phase: Evidence for a role in the maintenance of silencing. *Cell* **129**, 693–706 (2007). Medline doi:10.1016/j.cell.2007.03.036

44. I. Müller, S. Boyle, R. H. Singer, W. A. Bickmore, J. R. Chubb, Stable morphology, but dynamic internal reorganisation, of interphase human chromosomes in living cells. *PLoS ONE* **5**, e11560 (2010). Medline doi:10.1371/journal.pone.0011560

45. J. R. Chubb, W. A. Bickmore, Considering nuclear compartmentalization in the light of nuclear dynamics. *Cell* **112**, 403–406 (2003). Medline doi:10.1016/S0092-8674(03)00078-3

46. M. Hochstrasser, D. Mathog, Y. Gruenbaum, H. Saumweber, J. W. Sedat, Spatial organization of chromosomes in the salivary gland nuclei of Drosophila

melanogaster. *J. Cell Biol.* **102**, 112–123 (1986). Medline doi:10.1083/jcb.102.1.112

47. W. F. Marshall, Order and disorder in the nucleus. *Curr. Biol.* **12**, R185–R192 (2002). Medline doi:10.1016/S0960-9822(02)00724-8

48. W. A. Bickmore, B. van Steensel, Genome architecture: Domain organization of interphase chromosomes. *Cell* **152**, 1270–1284 (2013). Medline doi:10.1016/j.cell.2013.02.001

49. J. H. Gibcus, J. Dekker, The hierarchy of the 3D genome. *Mol. Cell* **49**, 773–782 (2013). Medline doi:10.1016/j.molcel.2013.02.011